


Sensitivity of Quantum-Enhanced Interferometers

Dariya Salykina ^{1,2} and Farid Khalili ^{1,*} 

¹ Russian Quantum Center, Skolkovo 121205, Russia

² Faculty of Physics, Lomonosov Moscow State University, Moscow 119991, Russia

* Correspondence: farit.khalili@gmail.com

Abstract: We review various schemes of quantum-enhanced optical interferometers, both linear (SU(2)) and non-linear (SU(1,1)) ones, as well as hybrid SU(2)/SU(1,1) options, using the unified modular approach based on the Quantum Cramèr–Rao bound (QCRB), and taking into account the practical limitations pertinent to all real-world highly-sensitive interferometers. We focus on three important cases defined by the interferometer symmetry: (i) the asymmetric single-arm interferometer; (ii) the symmetric two-arm interferometer with the antisymmetric phase shifts in the arms; and (iii) the symmetric two-arm interferometer with the symmetric phase shifts in the arms. We show that while the optimal regimes for these cases differ significantly, their QCRBs asymptotically correspond to the same squeezing-enhanced shot noise limit (2), which first appeared in the pioneering work by C. Caves in 1981. We show also that in all considered cases the QCRB can be asymptotically saturated by the standard (direct or homodyne) detection schemes.

Keywords: interferometers; quantum noise; quantum Cramer-Rao bound

1. Introduction

Optical interferometers are an indispensable tool for many scientific and industrial applications; in particular, two famous interrelated examples worth mentioning here. In 1987, the Michelson interferometer (see Figure 1a) helped to disprove the ether theory [1], paving the way to A. Einstein’s special theory of relativity. After more than one century, the first direct observation of the gravitational waves [2] by the pair of LIGO interferometers [3] provided one of the most convincing proofs of A. Einstein’s general theory of relativity.

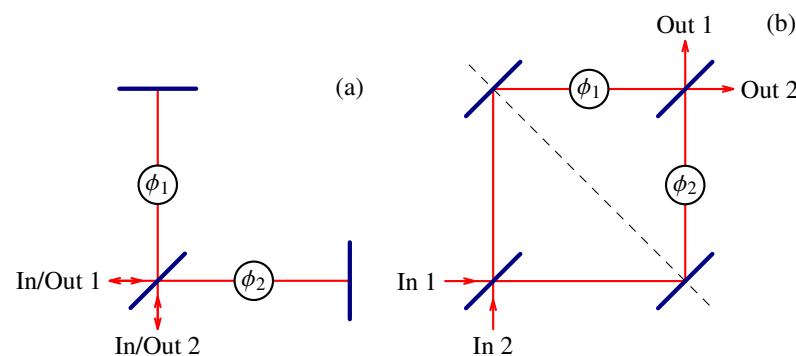


Figure 1. Michelson (a) and Mach–Zehnder (b) interferometers.

The sensitivity of the best modern interferometers is very high. Probably, they are the most sensitive measurement devices available now. For example, the contemporary laser interferometric gravitational-wave detectors, like LIGO and VIRGO [4], can measure relative elongations of their 3–4 km arms with the precision exceeding $\sim 10^{-23} \text{ Hz}^{-1/2}$ [5]. The major factor which limits their sensitivity is the quantum noise of the probing light. In



Citation: Salykina, D.; Khalili, F. Sensitivity of Quantum-Enhanced Interferometers. *Symmetry* **2023**, *15*, 774. <https://doi.org/10.3390/sym15030774>

Academic Editors: Polina Sharapova and Wiesław Leoński

Received: 12 January 2023

Revised: 8 March 2023

Accepted: 17 March 2023

Published: 22 March 2023



Copyright: © 2023 by the authors. Licensee MDPI, Basel, Switzerland. This article is an open access article distributed under the terms and conditions of the Creative Commons Attribution (CC BY) license (<https://creativecommons.org/licenses/by/4.0/>).

the most basic case of a coherent quantum state of light, the corresponding limit is known as the shot-noise one (SNL):

$$\Delta\phi_{\text{SNL}} = \frac{1}{2\sqrt{N}}, \quad (1)$$

where N is the mean number of photons interacting with the phase-shifting object(s), and ϕ is the measured phase.

This limit suggests a straightforward way of improving the phase sensitivity, namely the increase of N . However, there are important cases where this brute-force approach can not be used. In particular, in the laser gravitational-wave detectors, the circulating optical power reaches hundreds of kilowatts and is limited by various undesired nonlinear effects, like thermal distortions of the mirror shape or optomechanical parametric excitation [6,7]. Another example is the biological measurements [8], where the probing light intensity could be limited due to the fragility of the samples.

At the same time, it is known that the limit (1) can be overcome using more sophisticated “non-classical” quantum states. Accounting for the contemporary technological limitations, the simplest and the only practical class of such states consists of the Gaussian quadrature-squeezed states, which differ from the coherent ones by decreasing by e^{-r} (where r is the logarithmic squeeze factor) the uncertainty of one of its two quadratures and proportionally increased uncertainty of another one [9]. It was shown in the pioneering work by C. Caves [10], that in the realistic case of moderate squeezing, $e^{2r} \ll N$, the phase sensitivity could be improved by the factor e^{-r} :

$$\Delta\phi_{\text{SQZ}} \approx \frac{e^{-r}}{2\sqrt{N}}. \quad (2)$$

(the “squeezing-enhanced SNL”). In the hypothetical opposite case of very strong squeezing, $e^{2r} \sim N$, the phase sensitivity could approach the so-called Heisenberg limit (HL) [11–17], which, in the asymptotic case of $N \gg 1$, can be presented as follows:

$$\Delta\phi_{\text{HL}} \sim \frac{1}{N}. \quad (3)$$

The SNL (1) can be overcome also using Fock states and various other exotic non-Gaussian quantum states, see e.g., Refs. [11,18–25] and the reviews [26,27]. In Ref. [28], sensitivity approaching the HL (for a small N) was demonstrated experimentally using a non-Gaussian quantum state. However, the generation of these states with $N \gg 1$ is problematic with the current state-of-the-art technologies. Moreover, it was shown in Refs. [29,30], that in the important case of a symmetric interferometer with 50%/50% input beamsplitter(s), the optimal sensitivity could be provided by the Gaussian squeezed states.

The first proof-of-principle experiments with squeezed-light-enhanced interferometers were done in 1987 [31,32]. During the last years, squeezing up to 15 db was demonstrated experimentally [33–41]. Since 2011, the relatively small gravitational-wave detector GEO-600 routinely operates in the “squeezed” regime [42]. In 2019 the squeezing was implemented also in the larger and more sensitive detectors Advanced LIGO [5] and Advanced VIRGO [43], improving their sensitivity by about 3 dB; see also the review [44]. More impressive gain of about 10 dB is planned for the proposed third-generation detectors: Einstein Telescope [45] and Cosmic Explorer [46].

The main factor which limits the gain promised by the non-classical light is the optical losses. The non-Gaussian states, like the Fock or NOON ones, are most readily destroyed by them [47]. The Gaussian squeezed states are more robust. But nevertheless, in their case, the losses also significantly limit the sensitivity. As it was shown in Ref. [48], in the presence of losses, the gain provided by the squeezing reduces to

$$e^{-2r} \rightarrow e^{-2r} + \epsilon^2, \quad (4)$$

where

$$\epsilon^2 = \frac{1 - \eta}{\eta} \quad (5)$$

and η is the overall quantum efficiency of the interferometer.

The standard topologies of the Michelson and Mach–Zehnder interferometers used in the high-precision phase measurements are shown in Figure 1a,b, respectively. Evidently, the scheme of Figure 1b can be reduced to the one of Figure 1a by folding along the dashed line. Therefore, the Michelson interferometer is equivalent to the particular case of the Mach–Zehnder one with identical input and output beamsplitters. In Ref. [49], the term “SU(2) interferometer” was coined for them because the transformations of the two optical modes by the passive beamsplitters, as well as the antisymmetric phase shifts in the interferometer arms, are described by 2×2 complex matrices belonging to the group SU(2).

In the standard operating regime of the SU(2) interferometers, one of the input ports (the bright one) is excited by the laser light. Within the idealized theoretical treatment, this corresponds to the injection of a coherent quantum state into this port. The second port either remains dark, or the squeezed vacuum is fed into it, as it was proposed in Ref. [10]. Evidently, other combinations with a coherent, squeezed vacuum or squeezed coherent quantum states being injected into one or both input ports are possible, see e.g., Refs. [30,50–53] and the review [54].

In 1986, a novel scheme of the so-called SU(1,1) interferometer was proposed by Yurke et al. [49], see Figure 2. The key elements here are two optical parametric amplifiers (OPA), which replace the beamsplitters used in the SU(2) interferometer. The OPAs could be either degenerate ones (DOPA), that is, with the signal and idler beams being identical, or non-degenerate ones (NOPA), with the physically separated signal and idler beams. The name “SU(1,1) interferometer” is due to the fact that the transformations of the optical modes by parametric amplifiers, as well as the symmetric (relevant to this kind of interferometer) phase shifts in the interferometer arms, are described by 2×2 complex matrices belonging to the group SU(1,1). In Refs. [55,56], SU(1,1) interferometers with the sensitivity exceeding the SNL by 3–4 db were demonstrated experimentally.

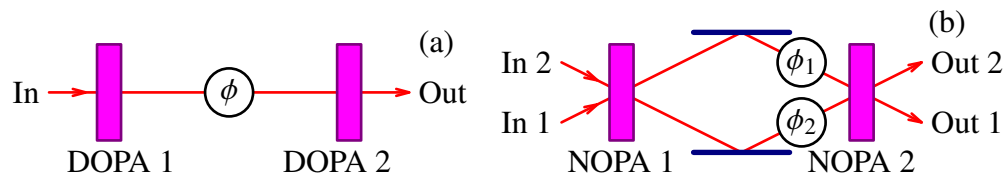


Figure 2. Single-arm (a) and two-arm (b) SU(1,1) interferometers. DOPA 1,2: degenerate optical parametric amplifiers; NOPA: nondegenerate optical parametric amplifiers.

At first sight, the non-degenerate version shown in Figure 2b looks very similar to the Mach–Zehnder interferometer (Figure 1b), with the input and output squeezers playing the role of the respective beamsplitters. However, this visual similarity is misleading. Opposite to the SU(2) interferometers, the non-degenerate SU(1,1) one is sensitive only to the sum phase shift $\phi_1 + \phi_2$ in the arms relative to the parametric pump phase, see Section 5.5.

Later, several enhancements to this scheme were proposed. In particular, it was shown that the performance of an SU(1,1) interferometer could be improved by seeding it with coherent or Fock quantum states [57–60]. In Ref. [61], the Fock states seeded SU(1,1) interferometer was demonstrated experimentally.

In Ref. [62], various detection options for the SU(1,1) interferometer were considered, and the new scheme of the truncated SU(1,1) interferometer, with the second OPA replaced by two homodyne detectors, was proposed and demonstrated in the experiment. In Ref. [63], the evolution of the Wigner function [64] in the SU(1,1) interferometer was calculated. In Ref. [65], the nonlinear SU(1,1) interferometer and the hybrid “seminonlinear” one were demonstrated experimentally.

Reviews of various topologies and implementations of the SU(1,1) interferometers can be found in Refs. [66–68].

The generalized conceptual schemes of the interferometric phase measurements, which encompass both SU(2) and SU(1,1) options, are presented in Figure 3. Two configurations are shown: (a) with the unknown (signal) phase shift ϕ introduced into one arm only (the single-arm interferometer), and (b) with the two-phase shifts ϕ_1 and ϕ_2 introduced respectively into each of the arms (the two-arm one). In both cases, the left block prepares the initial single- or two-mode quantum state $|\psi\rangle$ of the probing light. Then the light experiences the phase shift(s) and, after that, is measured by the right block. In the single-arm case, evidently, a second beam providing the phase reference is necessary. It could correspond to the local oscillator beam of the homodyne detector in the SU(2) interferometer case or to the double-frequency pump for the second OPA in the SU(1,1) one. In the two-arm case, the reference beam is optional: it is required only if the sum phase shift $\phi_1 + \phi_2$ has to be measured.

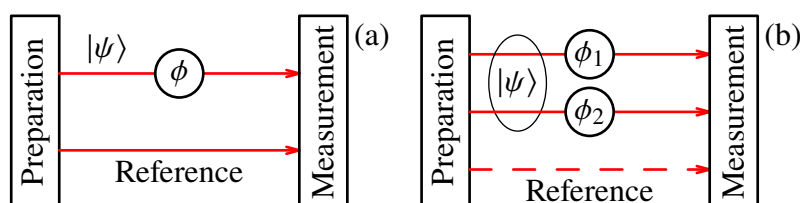


Figure 3. Conceptual schemes of the single-arm (a) and two-arm (b) interferometers. $|\psi\rangle$: single- or two-mode quantum state of the probing light.

Joint optimization of the preparation and measurement blocks can be a tedious task. In order to simplify it, an approach based on the quantum Cramèr–Rao bound (QCRB) [69] is broadly used in the literature, see e.g., reviews [26,54,67] and the references therein. The QCRB defines the ultimate sensitivity achievable for any given initial quantum state $|\psi\rangle$. Therefore, it allows the optimization of the preparation block independently of the measurement block. Then, any measurement which saturates the QCRB automatically will be an optimal one.

The QCRB could be explained in the following way (we would like to emphasize that this approach actually is not rigorous and can be used only for heuristic purposes). Start with the (hypothetical) Heisenberg uncertainty relation for the phase $\hat{\phi}$ and photons number \hat{N} for the initial quantum state of the probing light $|\psi\rangle$ [70]:

$$\Delta N \Delta \phi \geq \frac{1}{2}. \tag{6}$$

Evidently, the phase uncertainty $\Delta\phi$ defines the ultimate sensitivity limit achievable for a given $|\psi\rangle$. In particular, in the coherent state case with $\Delta N = \sqrt{N}$ we obtain Equation (1). Squeezing of the phase quadrature proportionally increases ΔN , giving Equation (2). The Heisenberg limit (3) arises from the (strictly speaking, incorrect) argument that ΔN can not exceed N .

It is known, however, that a Hermitian phase operator $\hat{\phi}$, conjugate to the number of quanta operator \hat{N} , does not exist and therefore, the “regular” Heisenberg uncertainty relation of form (6) also does not exist [71,72]. Various ways to circumvent this problem were proposed [73–75]. At the same time, the QCRB for the particular case of the interferometric phase measurement can be expressed in the form identical to (6), see details in Section 3. But in this case, ϕ has the meaning of a c -number shift of the probing light phase created by some external agent (for example, a displacement of the interferometer mirror(s)), while ΔN is still the photon number uncertainty of the probing light.

The goal of this review is to provide the *unified* view on the *practical* configurations of the quantum-enhanced interferometers based on the QCRB. The “unified” here means that we analyze both the single- and two-arm interferometers and, for each case, both SU(2) and SU(1,1) preparation and measurement options. For all configurations, we optimize first the preparation block using the QCRB. Then we identify measurement procedures that could saturate it.

“Practical” means the following limitations. (i) We focus on the high-precision measurements with $\Delta\phi \ll 1$, because, in the opposite case, the required sensitivity can be easily obtained using the coherent state. (ii) We consider only the Gaussian quantum states because technologies of preparation of bright (multi-photon) Gaussian states, in contrast to the exotic non-Gaussian states, are well developed and refined. (iii) We limit ourselves to standard and well-developed detection schemes. (iv) We take into account that the useful amount of squeezing is limited by the optical losses in the interferometer; see Equation (4). Assuming the realistic values of $\epsilon^2 \gtrsim 10^{-2}$, this means that the strong classical (coherent state) pumping with

$$|\alpha|^2 \approx N \gg e^{2r}, \quad (7)$$

where α is the classical amplitude, is obligatory for the high-precision phase measurements. Due to this limitation, we do not consider the Heisenberg limit here.

The detailed analysis of optical losses introduced by all elements in all the schemes considered here far exceeds the scope of this work. At the same time, in state-of-the-art interferometers and, in particular, in laser gravitational-wave detectors, the main part of the total loss budget is constituted by losses in the output optical path, including the photodetectors’ quantum inefficiency (the external losses), see e.g., Refs. [42,76]. We take into account only this kind of loss. This approach significantly simplifies the equations while providing realistic practical sensitivity estimates.

This paper is organized as follows. In the next section, we discuss the symmetry features of the configurations shown in Figure 2. In Section 3 we, following Ref. [69], present the convenient uncertainty-relation-type form of the QCRB. Then in Sections 4 and 5, we analyze the sensitivity of the single-arm and two-arm interferometers, respectively, following the formulated above approach. In Section 6, we summarize the main results of this paper.

The appendices contain all the calculations that are not as necessary for an understanding of the main concepts discussed in this work.

2. Symmetry of the Interferometer

In the single-arm interferometer case shown in Figure 3, the reference beam does not interact with the phase-shifting object. Therefore, much stronger optical power can be sent into this beam, in comparison with the power in the probe beam, improving the sensitivity for a given optical power at the object (see discussion at the end of Section 3.1). Therefore, this configuration is, in essence, an *asymmetric* one.

Concerning the two-arm interferometer, in the vast majority of applications, the main goal is not to measure two phase shifts $\phi_{1,2}$ in the arms independently, but to measure instead the *antisymmetric* (differential) phase shift

$$\phi_- = \frac{\phi_1 - \phi_2}{2}. \quad (8a)$$

In principle, in presence of the reference beam, the *symmetric* (common) phase

$$\phi_+ = \frac{\phi_1 + \phi_2}{2}, \quad (8b)$$

also can be measured.

Note that typically in literature another normalization $\phi_{\pm} = \phi_1 \pm \phi_2$ is used, which enforces the factor 1/2 in Equation (22) instead in order to preserve the condition (23), see e.g., Refs. [52,77]. We, following Ref. [16], prefer to use the normalization (8) and (22) because it gives the final equations for the form more consistently between the single- and two-arm cases.

In the laser gravitational-wave detectors, the information about ϕ_+ is used for locking the common mode of the interferometer [6]. Another interesting example is the experimental proposals aimed at the preparation of the entangled quantum state of two mirrors [78–80]. However, due to vulnerability to various non-fundamental noise sources,

in particular to the laser technical noise, ϕ_+ typically is measured with a precision significantly inferior to the one of ϕ_- .

In the literature, when analyzing the two-arm interferometers, the asymmetric case with the signal phase shift in one arm only:

$$\phi_1 = \varphi, \quad \phi_2 = 0. \tag{9}$$

is often considered, implicitly assuming that it is equivalent to the antisymmetric one with the same value of ϕ_- :

$$\phi_1 = \varphi/2, \quad \phi_2 = -\varphi/2. \tag{10}$$

This case looks identical to the single-arm interferometer; compare Figure 1b for the case of $\phi_2 = 0$ and Figure 4a.

However, it was shown in Refs. [77,81] that in general, the cases of (9) and (10) do not provide the same sensitivity, see details in Section 5.2. Moreover, it was shown in Ref. [82] that in the case of (10), the symmetric balanced configuration of the interferometer with the equal values of the optical power in both arms is optimal, opposite to the real single-arm case.

Therefore, in this paper, we focus on the following three cases: (i) the *asymmetric* single-arm interferometer, (ii) the symmetric two-arm interferometer with the *antisymmetric* phase shifts in the arms, and (iii) the symmetric two-arm one with the *symmetric* phase shifts in the arms.

3. Quantum Cramèr–Rao Bound for Phase Measurements

3.1. General Case

Let us consider some quantum system, e.g., an optical field in the interferometer arms, in a state described by the density operator $\hat{\rho}$. Let $\hat{\rho}$ depend on $J \geq 1$ parameters $\phi_1, \phi_2 \dots, \phi_J$ which have to be estimated. Let

$$\mathbb{B} = \|\langle \delta\phi_j \delta\phi_k \rangle\| \tag{11}$$

($j, k = 1 \dots J$) be the covariance matrix of the estimates $\tilde{\phi}_j$ of ϕ_j , with

$$\delta\phi_j = \tilde{\phi}_j - \phi_j. \tag{12}$$

It was shown by C. Helstrom [69] that for any measurement procedure, \mathbb{B} satisfies the following quantum Cramèr–Rao inequality

$$\mathbb{B} \geq \mathbb{A}^{-1}, \tag{13}$$

where

$$\mathbb{A} = \left\| \frac{1}{2} \text{Tr}[\hat{\rho}(\hat{L}_j \hat{L}_k + \hat{L}_k \hat{L}_j)] \right\| \tag{14}$$

is the *quantum Fisher information* matrix and \hat{L}_j are the symmetrized logarithmic derivatives of $\hat{\rho}$, defined by

$$\frac{\partial \hat{\rho}}{\partial \phi_j} = \frac{1}{2}(\hat{\rho} \hat{L}_j + \hat{L}_j \hat{\rho}). \tag{15}$$

In Sec.VIII.4(c) of the book [69], the specific case of a displacement parameter ϕ estimation was considered. In this case,

$$\hat{\rho} = \hat{U} \hat{\rho}_0 \hat{U}^\dagger, \tag{16}$$

where ρ_0 is the initial state of the system,

$$\hat{U} = e^{-i\hat{N}\phi} \tag{17}$$

is the displacement operator, and \hat{N} is the infinitesimal generator of the displacement group. If ϕ is a c -number shift in the optical mode phase created by some external agent, then \hat{N} is the photon number operator of this mode. It was shown that in this case, if the quantum state $\hat{\rho}_0$ is pure for all values of ϕ ,

$$\hat{\rho} = |\psi\rangle\langle\psi|, \tag{18}$$

then inequality (13) reduces to Equation (6), with ΔN being the uncertainty of \hat{N} in the quantum state $|\psi\rangle$ and $\Delta\phi$ having the meaning of the phase estimation error.

Here we generalize this result to the multi-dimensional case. Let $\phi_1, \phi_2 \dots$ be the phase shifts introduced in the respective arms of the interferometer. In this case, the density operator $\hat{\rho}_0$ corresponds to the optical field state before the phase shifts (i.e., just after the first beamsplitter), and the evolution operator \hat{U} has the following form:

$$\hat{U} = \exp\left(-i \sum_{j=1}^J \hat{N}_j \phi_j\right) \tag{19}$$

with \hat{N}_j being the photon number operators of the respective arms of the interferometer. Note that they commute with each other:

$$\forall j, k: [\hat{N}_j, \hat{N}_k] = 0. \tag{20}$$

It is shown in Appendix A that in this commutative case, the quantum Fisher information matrix is proportional to the variances matrix of the operators \hat{N}_j :

$$\mathbb{A} = 4 \|\langle \delta \hat{N}_j \delta \hat{N}_k \rangle\|; \tag{21}$$

through the paper, we denote $\delta \hat{Q} = \hat{Q} - \langle \hat{Q} \rangle$ for any operator \hat{Q} .

Concluding this subsection, we would like to emphasize one actually trivial but important issue. The sensitivity limits (6) and (13), and therefore (1)–(3) are defined in terms of the photon number statistics *at the phase shifting object(s)*, that is in the interferometer arm(s). At the same time, in the literature, they often are expressed in terms of the incident photon numbers, that is, of the photon numbers at the interferometer input ports. The latter approach, while technically correct, usually leads to more cumbersome final equations and sometimes misleading statements. In particular, in SU(1,1) interferometers, the incident light is amplified by the input NOPA and therefore, the equation for the phase measurement error, being expressed in terms of the incident photon numbers, contains the amplification factor. Due to this reason, this equation could look like exceeding the HL, which is actually not the case in the strict sense of Equation (3).

We would like to mention also again that in the most high-power contemporary interferometers, namely the laser interferometric gravitational-wave detectors, the optical power in the arms is limited not by the pump laser power but by the nonlinear effects inside the interferometer. Therefore, in addition to the consistency with QCRB and to its mathematical cleanness, the approach which is based on photon number statistics the phase shifting object(s) can be considered more practical. Due to these reasons, we will follow it in this work.

3.2. Differential and Common Modes

Consider now particular case of $J = 2$ which the most relevant to the interferometers. Following Section 2, let us rewrite the QCRB directly in terms of the common and differential phase shifts (8). Introduce the corresponding common and differential values of the photon number in the interferometer:

$$\hat{N}_{\pm} = \hat{N}_1 \pm \hat{N}_2. \tag{22}$$

Note that the evolution operator (19), expressed in terms of ϕ_{\pm} and \hat{N}_{\pm} , retains its form:

$$\hat{U} = e^{-i(\hat{N}_1\phi_1 + \hat{N}_2\phi_2)} = e^{-i(\hat{N}_+\phi_+ + \hat{N}_-\phi_-)}. \tag{23}$$

Therefore, the QCRB for ϕ_{\pm} also has the form (13), up to the evident modification of the notations (compare with Equations (4)–(6) of Ref. [29]):

$$\mathbb{B} = \begin{pmatrix} \langle(\delta\phi_+)^2\rangle & \langle\delta\phi_+ \delta\phi_-\rangle \\ \langle\delta\phi_+ \delta\phi_-\rangle & \langle(\delta\phi_-)^2\rangle \end{pmatrix}, \tag{24a}$$

$$\mathbb{A} = 4 \begin{pmatrix} \langle(\delta\hat{N}_+)^2\rangle & \langle\delta\hat{N}_+ \delta\hat{N}_-\rangle \\ \langle\delta\hat{N}_+ \delta\hat{N}_-\rangle & \langle(\delta\hat{N}_-)^2\rangle \end{pmatrix}, \tag{24b}$$

where

$$\delta\phi_{\pm} = \tilde{\phi}_{\pm} - \phi_{\pm}. \tag{25}$$

The explicit form of the inverse Fisher information matrix can be readily found in this case:

$$\mathbb{A}^{-1} = \frac{1}{4 \text{Det}} \begin{pmatrix} \langle(\delta\hat{N}_-)^2\rangle & -\langle\delta\hat{N}_+ \delta\hat{N}_-\rangle \\ -\langle\delta\hat{N}_+ \delta\hat{N}_-\rangle & \langle(\delta\hat{N}_+)^2\rangle \end{pmatrix}, \tag{26}$$

where

$$\text{Det} = \langle(\delta\hat{N}_+)^2\rangle\langle(\delta\hat{N}_-)^2\rangle - \langle\delta\hat{N}_+ \delta\hat{N}_-\rangle^2. \tag{27}$$

4. Single-Arm Interferometers

4.1. QCRB

Two configurations of the single-arm interferometers, the SU(2) and SU(1,1) ones, are shown in Figure 4a,b, respectively. In both cases, we assume that the incident light is prepared in the coherent state $|\alpha_0\rangle$. In the first case, the input beamsplitter BS 1 splits the incident beam into the probe and reference ones. The probe beam is squeezed by the degenerate optical parametric amplifier DOPA and then acquires the signal phase shift ϕ . Finally, its phase quadrature is measured by the phase-sensitive balanced homodyne detector, consisting of the output beamsplitter BS 2 and two photodetectors Det 1 and Det 2. The second (reference) beam, with its phase shifted by $\pi/2$, serves as the local oscillator for the homodyne detector.

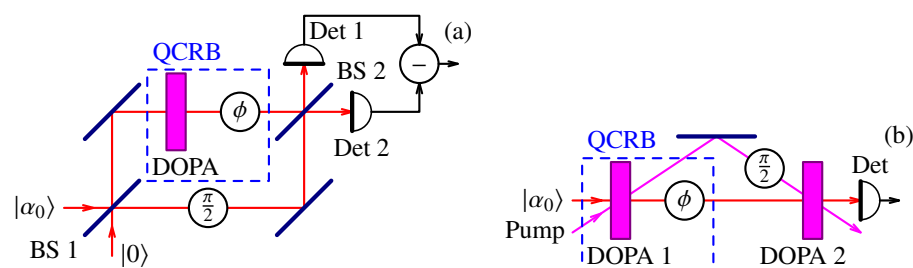


Figure 4. Single-arm SU(2) (a) and SU(1,1) (b) interferometers. BS: beamsplitters; DOPA: degenerate optical parametric amplifiers; Det: detectors. The part, common for both schemes, is enclosed into the dashed rectangle and labeled as “QCRB”.

Note the unusual placement of the squeezer DOPA. In the case of the standard placement (in the “south” input port of BS 1), squeezing in the probe beam would be diluted by the vacuum fluctuations entering the interferometer through the classical pump (“west”) port, thus degrading the sensitivity. The placement of the squeezer directly in the signal arm solves this problem. However, as we show here, the optimal sensitivity of this scheme corresponds to the highly unbalanced regime with the BS 1 transmissivity $T \rightarrow 1$. It is easy to see that, in this case, the squeezer could be moved to its standard place without the sensitivity degradation.

In the SU(1,1) case, the incident beam goes directly to the squeezer DOPA 1, then acquires the signal phase shift ϕ , and finally is anti-squeezed by the second parametric

amplifier DOPA 2, excited by the same pump beam as the first one, but with the phase shifted by $\pi/2$ (which corresponds to inversion of the squeeze factor sign). In this case, the pump beam serves as the phase reference, allowing the use of the simple direct detection method instead of the homodyne one.

It is easy to see that these schemes differ only by the measurement methods, while the preparation and the phase shift parts that are relevant to the QCRB (in Figure 4 they are enclosed into dashed rectangles and marked as “QCRB”) are identical. Therefore, both schemes are characterized by the same Cramèr–Rao limit (6), where ΔN is the uncertainty of the photon number $\hat{N} = \hat{a}^\dagger \hat{a}$ in the squeezed coherent state generated by DOPA/DOPA 1 and \hat{a}, \hat{a}^\dagger are the corresponding annihilation and creation operators.

In the Heisenberg picture, the operator \hat{a} can be expressed as follows:

$$\hat{a} = \alpha + \hat{z} \cosh r + \hat{z}^\dagger e^{2i\theta} \sinh r, \tag{28}$$

where α is the classical amplitude of the probe beam at the phase shifting object, \hat{z}, \hat{z}^\dagger are the annihilation and creation operators of the input vacuum fluctuations of DOPA/DOPA 1, $r > 0$ is the squeeze factor, and θ is the squeeze angle. We assume here without limiting the generality that $\arg \alpha = 0$ (this assumption just defines the reference point for all phases).

It follows from Equation (28) that

$$\langle (\delta \hat{N})^2 \rangle = \alpha^2 (\cosh 2r + \sinh 2r \cos 2\theta) + \frac{1}{2} \sinh^2 2r. \tag{29}$$

The maximum of this expression is provided by

$$\theta = 0. \tag{30}$$

This value of θ corresponds to the anti-squeezing of the amplitude quadrature (the one which is in phase with the classical carrier) and to the proportional squeezing of the phase quadrature. The resulting QCRB has the following form:

$$\langle (\delta \phi)^2 \rangle = \frac{1}{4 \langle (\delta \hat{N})^2 \rangle} = \frac{1}{4(\alpha^2 e^{2r} + \frac{1}{2} \sinh^2 2r)}. \tag{31}$$

4.2. Homodyne Detection

Here we take into account explicitly the homodyne detector and the corresponding reference beam. It is well known that in the homodyne detection-based schemes, the sensitivity for a given optical power at the object monotonously improves with the increase of the local oscillator power. Therefore, here we consider the general case of the unbalanced beamsplitter BS 1 with the power transmissivity $T \neq 1/2$.

The annihilation operators of, respectively, the probe and the reference beams just before the output beamsplitter BS 2 (see Figure 4a) are the following:

$$\hat{c} = \hat{a} e^{-i\phi}, \tag{32a}$$

$$\hat{c}_R = i\alpha_R + \hat{a}_R, \tag{32b}$$

where α_R , with $\arg \alpha_R = 0$, is the classical amplitude of the reference beam, the factor i takes into account the phase shift $\pi/2$ in the reference arm, and the annihilation operator \hat{a}_R corresponds to a vacuum field. The balanced output beamsplitter transforms them as follows:

$$\hat{d}_{1,2} = \frac{\hat{c} \pm \hat{c}_R}{\sqrt{2}}. \tag{33}$$

Following Ref. [83], we model the losses by imaginary beamsplitters with the power transmissivities η , which mix the output fields with the vacuum noises $\hat{y}_{1,2}$:

$$\hat{f}_j = \sqrt{\eta} \hat{d}_j + \sqrt{1 - \eta} \hat{y}_j, \tag{34}$$

where $j = 1, 2$. Correspondingly, the measured differential number of quanta is equal to

$$\hat{n}_- = \hat{f}_1^\dagger \hat{f}_1 - \hat{f}_2^\dagger \hat{f}_2. \tag{35}$$

Combining Equations (28), (30), and (32)–(35), we obtain that the mean number and the variance of \hat{n}_- are equal to, respectively,

$$\langle \hat{n}_- \rangle = -2\eta\alpha\alpha_R \sin \phi, \tag{36a}$$

$$\langle (\delta \hat{n}_-)^2 \rangle = \eta^2 \alpha_R^2 (\cosh 2r - \sinh 2r \cos 2\phi + \epsilon^2) + \eta(\alpha^2 + \sinh^2 r). \tag{36b}$$

Using the standard error propagation formula:

$$\langle (\delta \phi)^2 \rangle = \frac{\langle (\delta \hat{n}_-)^2 \rangle}{G^2} \Big|_{\phi \rightarrow 0}, \tag{37}$$

where

$$G = \frac{\partial \langle \hat{n}_- \rangle}{\partial \phi} = -2\eta\alpha\alpha_R \cos \phi \tag{38}$$

is the gain factor, we obtain that

$$\langle (\delta \phi)^2 \rangle = \frac{1}{4} \left(\frac{e^{-2r} + \epsilon^2}{\alpha^2} + \frac{\alpha^2 + \sinh^2 r}{\eta\alpha^2\alpha_R^2} \right). \tag{39}$$

The term $\propto 1/\alpha_R^2$ in this equation, which originates from the quantum noise of the reference beam, vanishes in the strongly asymmetric case of $\alpha_R^2 \rightarrow \infty$ (which corresponds to $\alpha_0 \rightarrow \infty$, $T \rightarrow 1$, and $\alpha_0\sqrt{1-T} = \alpha$), giving

$$\langle (\delta \phi)^2 \rangle = \frac{e^{-2r} + \epsilon^2}{4\alpha^2}. \tag{40}$$

This value differs from the fundamental limit (31) by the losses term ϵ^2 and by the absence of the small term $\frac{1}{2} \sinh^2 2r$ in the denominator.

It was shown in Ref. [84], that the latter one arises because the mean value of \hat{n}_- does not contain full information about ϕ . Some of this information is contained in the higher momenta of \hat{n}_- and can be recovered using more sophisticated multi-shot Bayesian measurements, as it was proposed in [84]. However, in the case of (7), the ordinary homodyne measurement is sufficient.

4.3. SU(1,1) Measurement

Consider now the single-arm SU(1,1) interferometer, shown in Figure 4b. In this case, the phase dependence of the measured photon number \hat{n} is created by the DOPA 2, which performs the anti-squeezing operation

$$\hat{d} = \hat{c} \cosh R - \hat{c}^\dagger e^{2i\theta} \sinh R. \tag{41}$$

Here \hat{c} is given by Equation (32a), $R > 0$ is the anti-squeeze factor, and θ is the same squeeze angle as in Equation (28).

To take into account the losses, we use the same imaginary beamsplitter model as in the previous case, assuming that the measured photons number is equal to

$$\hat{n} = \hat{f}^\dagger \hat{f}, \tag{42}$$

where

$$\hat{f} = \sqrt{\eta} \hat{d} + \sqrt{1-\eta} \hat{y} \tag{43}$$

and \hat{y} is the vacuum noise introduced by the losses (compare with Equation (34)).

The mean value and variance of \hat{n} are calculated in Appendix B, see Equations (A9). Here we consider only the particular case of

$$e^{2R} \gg 1, \quad (44)$$

because (i) it significantly simplifies the equations while providing the sensitivity approaching the QCRB (31), and (ii) allows the suppression of influence of the photodetector inefficiency [16] (note that in the perfectly realistic case of the 10 dB squeezing, $e^{2R} = 10 \gg 1$). In this case,

$$\langle \hat{n} \rangle = \eta e^{2R} \left[\alpha^2 \sin^2(\theta + \phi) + \frac{|\sigma|^2}{4} \right], \quad (45a)$$

$$\langle (\delta \hat{n})^2 \rangle = \eta^2 \left\{ e^{4R} |\sigma|^2 \left[\alpha^2 \sin^2(\theta + \phi) + \frac{|\sigma|^2}{8} \right] + \epsilon^2 e^{2R} \left[\alpha^2 \sin^2(\theta + \phi) + \frac{|\sigma|^2}{4} \right] \right\}, \quad (45b)$$

where

$$|\sigma|^2 = \cosh 2r - \sinh 2r \cos 2\phi. \quad (46)$$

Using again the error propagation formula:

$$\langle (\delta \phi)^2 \rangle = \frac{\langle (\delta \hat{n})^2 \rangle}{G^2} \Big|_{\phi \rightarrow 0} \quad (47)$$

with

$$G = \frac{\partial \langle \hat{n} \rangle}{\partial \phi} = \eta e^{2R} \left[\alpha^2 \sin 2(\theta + \phi) + \frac{1}{2} \sinh 2r \sin 2\phi \right], \quad (48)$$

we obtain that

$$\begin{aligned} \langle (\delta \phi)^2 \rangle &= \frac{\langle (\delta \hat{n})^2 \rangle}{G^2} \Big|_{\phi \rightarrow 0} \\ &= \frac{1}{4\alpha^2 \cos^2 \theta} \left[e^{-2r} \left(1 + \frac{e^{-2r}}{8\alpha^2 \sin^2 \theta} \right) + \epsilon^2 e^{-2R} \left(1 + \frac{e^{-2r}}{4\alpha^2 \sin^2 \theta} \right) \right]. \end{aligned} \quad (49)$$

In the case of a small, but not non-zero squeeze angle:

$$\frac{e^{-2r}}{N} \ll \theta^2 \ll 1, \quad (50)$$

the measurement error is equal to:

$$\langle (\delta \phi)^2 \rangle = \frac{e^{-2r} + \epsilon^2 e^{-2R}}{4\alpha^2}. \quad (51)$$

This equation differs from the previous one (40) by the additional factor e^{-2R} which suppresses the sensitivity degradation imposed by the optical losses. Evidently, this advantage comes from the amplification of the signal in the second OPA. However, this advantage is not unique to the SU(1,1) interferometers. It was shown in Ref. [10] that a similar gain could be achieved in the SU(2) by using the additional NOPA(s) located before the photodetector(s). Applications of this idea to various configurations of interferometers, both SU(1,1) and SU(2) ones, were considered in Ref. [16]. Several years ago, the proof-of-principle experiments with SU(1,1) [85] and SU(2) [35] interferometers were done.

In the rest of this paper, we, for brevity, do not take the factor e^{2R} into account explicitly, absorbing it into ϵ^2 :

$$\epsilon^2 e^{-2R} \rightarrow \epsilon^2. \quad (52)$$

Up to this factor, in the asymptotic case of (7) both schemes shown in Figure 4 and considered in this section provide the same sensitivity. If the optical losses are sufficiently small (or suppressed by the parametric amplification):

$$\epsilon^2 \ll e^{-2r}, \tag{53}$$

then both schemes saturate the common for them QCRB (31) up to the small term $\frac{1}{2} \sinh^2 2r$.

5. Two-Arm Interferometers

5.1. QCRB

Two variants of the preparation block of the two-arm interferometer (see Figure 3b) are shown in Figure 5: the “SU(2)” (a) and the “SU(1,1)” (b) ones. Let us start with the first one.

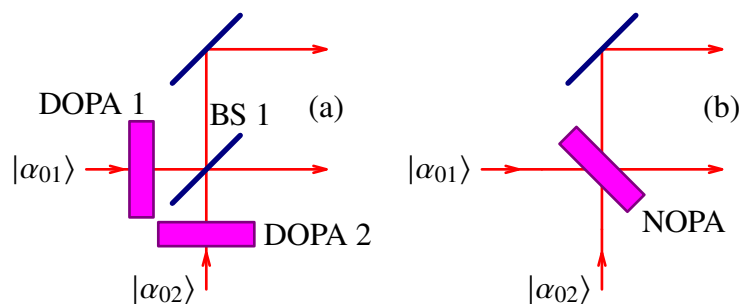


Figure 5. Preparation options for the two-arm interferometer shown in Figure 3b. (a): SU(2) interferometer; (b): SU(1,1) interferometer. BS 1: beamsplitters; DOPA 1,2: degenerate optical parametric amplifiers; NOPA: non-degenerate optical parametric amplifier.

We consider the most general case, assuming that both input ports of the beamsplitter BS 1 are excited by two squeezed coherent states generated by two degenerate parametric amplifiers DOPA 1,2. The annihilation operators describing these quantum states in the Heisenberg picture can be presented as follows ($j = 1, 2$):

$$\hat{a}_j = \alpha_j + \hat{z}_j \cosh r_j + \hat{z}_j^\dagger e^{2i\theta_j} \sinh r_j, \tag{54}$$

where α_j are the classical amplitudes, the operators \hat{z}_j correspond to vacuum fields, r_j are the squeeze factors and θ_j are the squeeze angles. After the input beamsplitter BS 1, correspondingly, we obtain:

$$\hat{b}_1 = \frac{\hat{a}_1 + \hat{a}_2}{\sqrt{2}}, \quad \hat{b}_2 = \frac{\hat{a}_1 - \hat{a}_2}{\sqrt{2}}, \tag{55}$$

In particular, the classical amplitudes of the beamsplitter output beams are equal to

$$\beta_1 = \frac{\alpha_1 + \alpha_2}{\sqrt{2}}, \quad \beta_2 = \frac{\alpha_1 - \alpha_2}{\sqrt{2}}. \tag{56}$$

Taking into account that the best sensitivity for the differential phase ϕ_- is provided by the balanced interferometer [82], we suppose that $|\beta_1| = |\beta_2|$. Then, without further limiting the generality (and setting thus the reference point for all phases), we assume that

$$\beta_{1,2} = \frac{\alpha e^{\pm i\zeta}}{\sqrt{2}}, \tag{57}$$

where $\arg \alpha = 0$ and 2ζ is the relative phase shift between β_1 and β_2 . It follows from Equation (56), that in this case,

$$\alpha_1 = \alpha \cos \zeta, \quad \alpha_2 = i\alpha \sin \zeta \tag{58}$$

and

$$|\beta_1|^2 + |\beta_2|^2 = |\alpha_1|^2 + |\alpha_2|^2 = |\alpha|^2. \tag{59}$$

Then it follows from Equation (55), that the common and differential values of the photon numbers at the phase-shifting objects are equal to

$$\hat{N}_+ = \hat{b}_1^\dagger \hat{b}_1 + \hat{b}_2^\dagger \hat{b}_2 = \hat{a}_1^\dagger \hat{a}_1 + \hat{a}_2^\dagger \hat{a}_2, \tag{60a}$$

$$\hat{N}_- = \hat{b}_1^\dagger \hat{b}_1 - \hat{b}_2^\dagger \hat{b}_2 = \hat{a}_1^\dagger \hat{a}_2 + \hat{a}_2^\dagger \hat{a}_1. \tag{60b}$$

The second momenta of these operators are calculated in Appendix C. In the particular case of (58), they can be presented as follows:

$$\langle (\delta \hat{N}_+)^2 \rangle = \alpha^2 (\sigma_{1+}^2 \cos^2 \zeta + \sigma_{2-}^2 \sin^2 \zeta) + \frac{1}{2} (\sinh^2 2r_1 + \sinh^2 2r_2), \tag{61a}$$

$$\begin{aligned} \langle (\delta \hat{N}_-)^2 \rangle &= \alpha^2 (\sigma_{1-}^2 \sin^2 \zeta + \sigma_{2+}^2 \cos^2 \zeta) \\ &+ \sinh^2(r_1 + r_2) \cos^2(\theta_1 - \theta_2) + \sinh^2(r_1 - r_2) \sin^2(\theta_1 - \theta_2), \end{aligned} \tag{61b}$$

$$\langle \delta \hat{N}_+ \delta \hat{N}_- \rangle = \frac{\alpha^2}{2} (\sinh 2r_1 \sin 2\theta_1 + \sinh 2r_2 \sin 2\theta_2) \sin 2\zeta, \tag{61c}$$

where

$$\sigma_{j\pm}^2 = \cosh 2r_j \pm \sinh 2r_j \cos 2\theta_j. \tag{62}$$

Consider now the following three characteristic scenarios.

5.1.1. Single Squeezer

Start with the case of a single squeezer. Just to be specific, we suppose that

$$r_1 = 0, \quad r_2 > 0. \tag{63}$$

It follows from Equations (61), that in this case,

$$\langle (\delta \hat{N}_+)^2 \rangle = \alpha^2 (\cos^2 \zeta + \sigma_{2-}^2 \sin^2 \zeta) + \frac{1}{2} \sinh^2 2r_2, \tag{64a}$$

$$\langle (\delta \hat{N}_-)^2 \rangle = \alpha^2 (\sin^2 \zeta + \sigma_{2+}^2 \cos^2 \zeta) + \sinh^2 r_2, \tag{64b}$$

$$\langle \delta \hat{N}_+ \delta \hat{N}_- \rangle = \frac{\alpha^2}{2} \sinh 2r_2 \sin 2\theta_2 \sin 2\zeta. \tag{64c}$$

Then recall that the measurement of ϕ_- has higher priority than the measurement of ϕ_+ . Therefore, evidently, the following parameters have to be used, which maximize the leading (proportional to α^2) term in Equation (64b):

$$\theta_2 = 0, \quad \zeta = 0. \tag{65}$$

In this case it follows from Equation (26) that

$$\langle (\delta \phi_+)^2 \rangle = \frac{1}{4(\alpha^2 + \frac{1}{2} \sinh^2 2r_2)}, \tag{66a}$$

$$\langle (\delta \phi_-)^2 \rangle = \frac{1}{4(\alpha^2 e^{2r_2} + \sinh^2 r_2)}, \tag{66b}$$

$$\langle \delta \phi_+ \delta \phi_- \rangle = 0, \tag{67}$$

Note that conditions (63) and (65) describe injection of the classical carrier into only one (bright) port ($\alpha_2 = 0$) and injection of the squeezed vacuum into the second (dark) one. This regime exactly corresponds to the canonical case of [10].

Note also that due to condition (67), the measurement imprecision of ϕ_- is disentangled from the one of ϕ_+ , which is typically contaminated by the technical noise. This useful feature is true also for the “two squeezers” and “SU(1,1) type preparation” cases considered below. For brevity, we will not mention it again and will omit the corresponding equations for $\langle \delta\phi_+ \delta\phi_- \rangle$.

5.1.2. Two Squeezers

Suppose now that both input ports are squeezed. It is natural to assume that both squeeze factors are limited by the same technological constraints and therefore $|r_1| \sim |r_2|$. In this case, the leading (proportional to α^2) terms in Equations (61a) and (61b) can be maximized simultaneously by either

$$r_1 \sim r_2 > 0, \quad \theta_1 = \theta_2 = 0, \quad \zeta = 0, \tag{68a}$$

or

$$r_1 \sim r_2 > 0, \quad \theta_1 = \theta_2 = \frac{\pi}{2}, \quad \zeta = \frac{\pi}{2}. \tag{68b}$$

Both these options actually are equivalent, up to the renumbering of the ports. Similar to the previous (single squeezer) case, they also correspond to the injection bright carrier into one of the ports and the injection of the squeezed vacuum into the second one. But this time, the light at the bright port is also squeezed.

To be specific, we consider the first option, which gives:

$$\langle (\delta\phi_+)^2 \rangle = \frac{1}{4[\alpha^2 e^{2r_1} + \frac{1}{2}(\sinh^2 2r_1 + \sinh^2 2r_2)]}, \tag{69a}$$

$$\langle (\delta\phi_-)^2 \rangle = \frac{1}{4[\alpha^2 e^{2r_2} + \sinh^2(r_1 + r_2)]}. \tag{69b}$$

Therefore, the bright port squeezer allows us to obtain the sub-SNL sensitivity also for the common phase.

5.1.3. SU(1,1)-Type Preparation

Finally, consider the input part of the SU(1,1) interferometer, see Figure 5b. In this case, the incident fields at the phase-shifting objects can be presented as follows:

$$\hat{b}_1 = \beta_1 + \hat{z}_+ \cosh r + \hat{z}_-^\dagger e^{2i\theta} \sinh r, \tag{70a}$$

$$\hat{b}_2 = \beta_2 + \hat{z}_- \cosh r + \hat{z}_+^\dagger e^{2i\theta} \sinh r, \tag{70b}$$

where \hat{z}_\pm correspond to the vacuum fields and we assume that β_j are still given by Equation (57). It is easy to see that up to the trivial substitution

$$\hat{z}_\pm \rightarrow \frac{\hat{z}_1 \pm \hat{z}_2}{\sqrt{2}}, \tag{71}$$

Equations (70) coincide with Equations (54) and (55) for the particular case of

$$r_1 = -r_2 = r, \tag{72a}$$

$$\theta_1 = \theta_2 = \theta. \tag{72b}$$

This means that the SU(1,1) type scheme of Figure 5b can be treated as a special case of the SU(2) scheme of Figure 5a with the particular choice of the squeeze factors given by (72). Therefore, we can reuse Equation (61). Combining them with Equation (72), we obtain that

$$\langle (\delta \hat{N}_+)^2 \rangle = \alpha^2 (\cosh 2r_2 - \sinh 2r_2 \cos 2\theta) + \sinh^2 2r_2, \tag{73a}$$

$$\langle (\delta \hat{N}_-)^2 \rangle = \alpha^2 (\cosh 2r_2 + \sinh 2r_2 \cos 2\theta). \tag{73b}$$

independently on ζ .

In this case, a trade-off is possible between the ϕ_+ and ϕ_- . In particular, if $r_2 > 0$ and $\theta = 0$, then we have the sensitivity overcoming the SNL for ϕ_- , but proportionally degraded for ϕ_+ :

$$\langle (\delta \phi_+)^2 \rangle = \frac{1}{4(\alpha^2 e^{-2r_2} + \sinh^2 2r_2)}, \tag{74a}$$

$$\langle (\delta \phi_-)^2 \rangle = \frac{1}{4\alpha^2 e^{2r_2}}. \tag{74b}$$

If $r > 0$ and $\theta = \pi/2$, then the situation is opposite:

$$\langle (\delta \phi_+)^2 \rangle = \frac{1}{4(\alpha^2 e^{2r_2} + \sinh^2 2r_2)}, \tag{75a}$$

$$\langle (\delta \phi_-)^2 \rangle = \frac{1}{4\alpha^2 e^{-2r_2}}. \tag{75b}$$

However, the latter case hardly has any practical sense.

The following interesting case is also worth mentioning:

$$\theta = \frac{\pi}{4}, \tag{76}$$

which, similar to the two squeezers case, see Equation (69), also allows us to overcome the SNL for both ϕ_+ and ϕ_- simultaneously, but to a lesser degree:

$$\langle (\delta \phi_+)^2 \rangle = \frac{1}{4(\alpha^2 \cosh 2r_2 + \sinh^2 2r_2)}, \tag{77a}$$

$$\langle (\delta \phi_-)^2 \rangle = \frac{1}{4\alpha^2 \cosh 2r_2}. \tag{77b}$$

5.2. Measurement of Individual Phase Shifts in the Arms

Here we analyze the measurement precision $\langle (\delta \phi_{1,2})^2 \rangle$ for the individual phase shifts in the arms

$$\phi_{1,2} = \phi_+ \pm \phi_-. \tag{78}$$

In general, in order to recover them, both ϕ_+ and ϕ_- have to be measured. The measurement of ϕ_+ , in turn, requires a detection scheme that uses an additional (third) phase reference beam, e.g., the homodyne detector.

The values of measurement errors $\langle (\delta \phi_{1,2})^2 \rangle$ crucially depend on a priori information on $\phi_{1,2}$. It follows from Equations (67) and (78) that in the absence of this information, the mean square measurement errors of ϕ_+ and ϕ_- add up to

$$\langle (\delta \phi_{1,2})^2 \rangle = \langle (\delta \phi_+)^2 \rangle + \langle (\delta \phi_-)^2 \rangle, \tag{79}$$

where $\langle (\delta \phi_{\pm})^2 \rangle$ are given by Equations (66), (69) or (74), depending on the input state preparation procedure.

At the same time, suppose that an unknown phase shift φ is introduced into one, say, the first, arm only and the phase shift in another arm is known—say, equal to zero, see Equation (9). It follows from Equation (8), that in this asymmetric case,

$$\phi_+ = \phi_- = \frac{\varphi}{2}. \tag{80}$$

This means that both the “+” and the “−” channels carry the same information on φ . It is easy to show that in this case, with account for condition (67), the Fisher information values for both channels are summed:

$$\langle(\delta\varphi)^2\rangle = \frac{4}{1/\langle(\delta\phi_+)^2\rangle + 1/\langle(\delta\phi_-)^2\rangle}. \tag{81}$$

Consider then the case of the antisymmetric distribution of the phase shifts; see Equation (10). It corresponds to

$$\phi_+ = 0, \quad \phi_- = \frac{\varphi}{2}. \tag{82}$$

In this case, the “+” channel does not provide any information on φ ; correspondingly,

$$\langle(\delta\varphi)^2\rangle = 4\langle(\delta\phi_-)^2\rangle. \tag{83}$$

Evidently, the additional phase reference is useless in this case.

It was shown in Ref. [77], that the asymmetric and antisymmetric cases are equivalent only within the class of detection schemes insensitive to the common phase. Equations (81) and (83) clearly show the reason for this. Indeed, the first one contains the Fisher information from the “+” channel, in addition to the “−” one. Taking into account that in the double squeezed input case, there could be $\langle(\delta\phi_+)^2\rangle \approx \langle(\delta\phi_-)^2\rangle$, the value of (81) could be twice as small as of (83). At the same time, consider the asymmetric case with the neglected common phase information (assuming, for example, that a detection scheme that does not employ the reference beam is used). In this case, putting in Equation (81) $\langle(\delta\phi_+)^2\rangle \rightarrow \infty$, we recover Equation (83).

In Ref. [81], the following no-go theorem has been proven: if one of the input ports of the two-arm interferometer is kept in the vacuum state, then in the antisymmetric case the sensitivity is limited by the SNL independently of the quantum state at the second port. At the same time, in the asymmetric case this no-go theorem does not hold. The origin of this peculiar limitation also can be seen in Equations (81) and (83). Indeed, consider Equation (69), assuming that $r_2 = 0$, which corresponds to the vacuum state at the second input port. In this case, ϕ_- can not be measured with a precision better than the SNL, but ϕ_+ still can. Due to this reason, in the antisymmetric case, the precision is limited by the SNL, see Equation (83). But in the asymmetric case, the SNL can be overcome due to the Fisher information provided by the “+” channel, see Equation (81).

5.3. Double Homodyne Detection

In this and the next two subsections, we consider three variants of the measurement block of the two-arm interferometer (see Figure 3b), shown in Figure 6: the double homodyne detection (a), the double direct detection (b), and the SU(1,1) type measurement (c). Here we start with the first one.

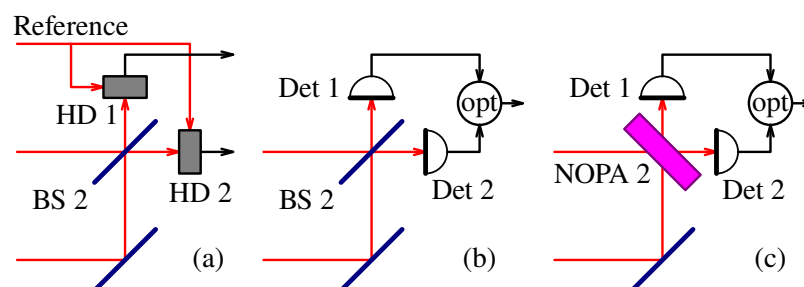


Figure 6. Measurement options for the two-arm interferometer shown in Figure 3b. (a): Double homodyne detection; (b): double direct detection; (c): SU(1,1) type measurement. BS 2: beamsplitter; NOPA 2: non-degenerate optical parametric amplifier; HD 1,2: homodyne detectors; Det 1,2: detectors; “opt” means the optimally weighted sum of the two outputs.

An evident advantage of the double homodyne detection scheme, in comparison with the more standard single homodyne detection one, as well as with the direct detection scheme considered in Section 5.4, is its ability to measure both the differential phase ϕ_- and (due to the external phase reference) the common phase ϕ_+ . Another probably more important advantage of homodyne detection in comparison with the direct one also could be mentioned here. The homodyne detectors can measure arbitrary quadrature of the output light of the interferometer; this feature is typically required by the schemes of overcoming the Standard Quantum Limit in optomechanical measurements, in particular, in the laser gravitational-wave detectors, see details in the reviews [86,87].

Let us continue the analysis of Section 5.1, see Equation (55), introducing the signal phase shifts in the arms ($j = 1, 2$):

$$\hat{c}_j = \hat{b}_j e^{-i\phi_j}. \tag{84}$$

The output beamsplitter BS 2 modifies them as follows:

$$\hat{d}_1 = \frac{\hat{c}_1 + \hat{c}_2}{\sqrt{2}}, \quad \hat{d}_2 = \frac{\hat{c}_1 - \hat{c}_2}{\sqrt{2}}. \tag{85}$$

Combining Equations (55), (84) and (85), and reusing Equation (34), we obtain that with account for the losses, the effective fields at the detectors are described by the annihilation operators

$$\hat{f}_1 = \sqrt{\eta}(\hat{a}_1 \cos \phi_- - i\hat{a}_2 \sin \phi_-)e^{-i\phi_+} + \sqrt{1-\eta} \hat{y}_1, \tag{86a}$$

$$\hat{f}_2 = \sqrt{\eta}(-i\hat{a}_1 \sin \phi_- + \hat{a}_2 \cos \phi_-)e^{-i\phi_+} + \sqrt{1-\eta} \hat{y}_2. \tag{86b}$$

Then, following the results of Section 5.1, we assume that

$$\hat{a}_1 = \alpha + \hat{z}_1 \cosh r_1 + \hat{z}_1^\dagger \sinh r_1, \tag{87a}$$

$$\hat{a}_2 = \hat{z}_2 \cosh r_2 + \hat{z}_2^\dagger \sinh r_2, \tag{87b}$$

where $\arg \alpha = 0$. Combining Equations (86) and (87) and taking into account that $|\alpha| \gg 1$ and $|\phi_\pm| \ll 1$, we obtain finally:

$$\hat{f}_1 = \sqrt{\eta}[\alpha(1 - i\phi_+) + \hat{z}_1 \cosh r_1 + \hat{z}_1^\dagger \sinh r_1] + \sqrt{1-\eta} \hat{y}_1, \tag{88a}$$

$$\hat{f}_2 = \sqrt{\eta}[-i\alpha\phi_- + \hat{z}_2 \cosh r_2 + \hat{z}_2^\dagger \sinh r_2] + \sqrt{1-\eta} \hat{y}_2. \tag{88b}$$

It follows from these equations, that the first (bright) output contains information about the common phase ϕ_+ , and the second (dark) one — about the differential one ϕ_- . Both could be measured independently by the respective homodyne detectors.

In order to calculate the measurement errors, it is convenient to introduce the sine quadratures of the input and output fields ($j = 1, 2$):

$$\hat{y}_j^s = \frac{\hat{y}_j - \hat{y}_j^\dagger}{i\sqrt{2}}, \quad \hat{z}_j^s = \frac{\hat{z}_j - \hat{z}_j^\dagger}{i\sqrt{2}}, \quad \hat{d}_j^s = \frac{\hat{d}_j - \hat{d}_j^\dagger}{i\sqrt{2}}. \tag{89}$$

In these notations, Equation (88) give:

$$\hat{f}_1^s = \sqrt{\eta}[-\sqrt{2}\alpha\phi_+ + \hat{z}_1^s e^{-r_1}] + \sqrt{1-\eta} \hat{y}_1^s, \tag{90a}$$

$$\hat{f}_2^s = \sqrt{\eta}[-\sqrt{2}\alpha\phi_- + \hat{z}_2^s e^{-r_2}] + \sqrt{1-\eta} \hat{y}_2^s. \tag{90b}$$

Taking into account that the variances of $\hat{y}_{1,2}^s$ and $\hat{z}_{1,2}^s$ are equal to 1/2, we obtain:

$$\langle (\delta\phi_+)^2 \rangle = \frac{e^{-2r_1} + \epsilon^2}{4\alpha^2}, \tag{91a}$$

$$\langle (\delta\phi_-)^2 \rangle = \frac{e^{-2r_2} + \epsilon^2}{4a^2}. \tag{91b}$$

In the asymptotic case of (7) and (53), these results are in the full agreement with the ones predicted by the QCRB, see Equations (66), (69) and (74).

5.4. Double Direct Detection

Consider now the double direct detection case, shown in Figure 6b. Using Equation (86), the photon numbers measured by the two photodetectors can be presented as follows:

$$\hat{n}_1^{\text{out}} = \hat{f}_1^\dagger \hat{f}_1 = \eta(\hat{n}_1 \cos^2 \phi_- + \hat{n}_2 \sin^2 \phi_- + \hat{Y} \cos \phi_- \sin \phi_-) + \hat{n}_1^{\text{loss}}, \tag{92a}$$

$$\hat{n}_2^{\text{out}} = \hat{f}_2^\dagger \hat{f}_2 = \eta(\hat{n}_1 \sin^2 \phi_- + \hat{n}_2 \cos^2 \phi_- - \hat{Y} \cos \phi_- \sin \phi_-) + \hat{n}_2^{\text{loss}}, \tag{92b}$$

where ($j = 1, 2$)

$$\hat{n}_j = \hat{a}_j^\dagger \hat{a}_j \tag{93}$$

are the incident photon numbers,

$$\hat{Y} = i(\hat{a}_2^\dagger \hat{a}_1 - \hat{a}_1^\dagger \hat{a}_2), \tag{94}$$

and

$$\hat{n}_j^{\text{loss}} = \sqrt{\eta(1-\eta)}(\hat{d}_j^\dagger \hat{y}_j + \hat{y}_j^\dagger \hat{d}_j) + (1-\eta)\hat{y}_j^\dagger \hat{y}_j \tag{95}$$

are the additional fluctuations created by the optical losses.

Correspondingly, the common and differential output photon numbers are equal to:

$$\hat{n}_+^{\text{out}} = \hat{n}_1^{\text{out}} + \hat{n}_2^{\text{out}} = \eta\hat{n}_+ + \hat{n}_1^{\text{loss}} + \hat{n}_2^{\text{loss}}, \tag{96a}$$

$$\hat{n}_-^{\text{out}} = \hat{n}_1^{\text{out}} - \hat{n}_2^{\text{out}} = \eta(\hat{n}_- \cos 2\phi_- + \hat{Y} \sin 2\phi_-) + \hat{n}_1^{\text{loss}} - \hat{n}_2^{\text{loss}}, \tag{96b}$$

where

$$\hat{n}_\pm = \hat{n}_1 \pm \hat{n}_2. \tag{97}$$

It is evident that in this case, due to the absence of the common phase reference, only the differential phase shift ϕ_- can be measured. Note also that \hat{n}_+ does not depend on ϕ_- . Due to this reason, in the literature, typically the measurement of the differential photons numbers \hat{n}_-^{out} only is considered, see e.g., Ref. [54]. However, fluctuations of \hat{n}_+^{out} and \hat{n}_-^{out} correlate. Therefore, the measurement of \hat{n}_+^{out} provides some information about the noise of \hat{n}_-^{out} , and taking this information into account by means of the optimal combination of both outputs, it is possible to improve the phase sensitivity [88]. The resulting measurement error can be presented as follows:

$$\langle (\delta\phi_-)^2 \rangle = \frac{1}{G^2} \left[\langle (\delta\hat{n}_-^{\text{out}})^2 \rangle - \frac{\langle \delta\hat{n}_-^{\text{out}} \delta\hat{n}_+^{\text{out}} \rangle^2}{\langle (\delta\hat{n}_+^{\text{out}})^2 \rangle} \right], \tag{98}$$

where

$$G = \frac{\partial \langle \hat{n}_-^{\text{out}} \rangle}{\partial \phi_-} \tag{99}$$

is the gain factor.

Here we, similarly to the double homodyne detection case (see Section 5.3), follow the results of Section 5.1, assuming that the incident fields are described by Equation (87). The explicit form of Equation (98) for this case is calculated in Appendix D, see Equation (A27).

Note that the squeeze factor r_1 is responsible for the common phase ϕ_+ sensitivity, see Section 5.1. Therefore, the “two squeezers” option has no sense in the direct detection case, which is insensitive to ϕ_+ . Consider the two remaining ones.

In the single squeezer case of Equation (63), Equation (A27) simplifies to

$$\langle (\delta\phi_-)^2 \rangle = \frac{1}{4(\alpha^2 - \sinh^2 r_2)^2} [\alpha^2 e^{-2r_2} + \sinh^2 r_2 + \epsilon^2 (\alpha^2 + \sinh^2 r_2) + 2(\sinh^2 2r_2 + 2\epsilon^2 \sinh^2 r_2) \cot^2 2\phi_- + O(\alpha^{-2})]. \tag{100}$$

In the SU(1,1)-type preparation case, see Equation (72a), we obtain:

$$\langle (\delta\phi_-)^2 \rangle = \frac{1}{4\alpha^4} [\alpha^2 e^{-2r_2} + \sinh^2 2r_2 + \epsilon^2 (\alpha^2 + 2\sinh^2 r_2) + 2(\sinh^2 2r_2 + 2\epsilon^2 \sinh^2 r_2) \cot^2 2\phi_- + O(\alpha^{-2})], \tag{101}$$

where $O(\alpha^{-2})$ means a value of the order of magnitude of $\alpha^{-2} \ll 1$.

In both cases, the terms diverging at $\phi_- \rightarrow 0$ can be suppressed by introducing a sufficiently big given constant displacement into ϕ_- . In the asymptotic case of (7), Equations (100) and (101) become identical to each other and to Equation (91b); that is, both homodyne and direct detection options provide the same asymptotic sensitivity for the differential phase.

5.5. SU(1,1) Measurement

Finally, consider the SU(1,1) measurement case, shown in Figure 6c. In this case, with account for Equation (84), the optical fields after the NOPA 2 can be presented as follows:

$$\hat{d}_1 = \hat{b}_1 e^{-i\phi_1} \cosh R + \hat{b}_2^\dagger e^{i(\phi_2+2i\theta)} \sinh R, \tag{102a}$$

$$\hat{d}_2 = \hat{b}_2 e^{-i\phi_1} \cosh R + \hat{b}_1^\dagger e^{i(\phi_2+2i\theta)} \sinh R \tag{102b}$$

where R, θ are, respectively, the squeeze factor and the squeeze angle of the NOPA 2. The corresponding output photon numbers are equal to

$$\hat{d}_1^\dagger \hat{d}_1 = \hat{b}_1^\dagger \hat{b}_1 \cosh^2 R + [\hat{b}_1^\dagger \hat{b}_2^\dagger e^{2i(\phi_++\theta)} + \hat{b}_1 \hat{b}_2 e^{-2i(\phi_++\theta)}] \cosh R \sinh R + \hat{b}_2 \hat{b}_2^\dagger \sinh^2 R, \tag{103a}$$

$$\hat{d}_2^\dagger \hat{d}_2 = \hat{b}_2^\dagger \hat{b}_2 \cosh^2 R + [\hat{b}_1^\dagger \hat{b}_2^\dagger e^{2i(\phi_++\theta)} + \hat{b}_1 \hat{b}_2 e^{-2i(\phi_++\theta)}] \cosh R \sinh R + \hat{b}_1 \hat{b}_1^\dagger \sinh^2 R. \tag{103b}$$

It follows from these equations that independently of the incident quantum state, this measurement procedure gives information only on the common phase ϕ_+ and, therefore, has no advantages in comparison with the single-arm SU(1,1) interferometer considered in Section 4.3.

In principle, sensitivity to the differential phase ϕ_- can be recovered by measuring the NOPA 2 outputs by means of the homodyne detectors. However, taking into account that the more simple SU(2)-type measurement schemes, considered in Sections 5.3 and 5.4, allow us to asymptotically saturate the QCRB, such a sophisticated scheme with two-phase references (NOPA pump and the homodyne detectors local oscillator beams) hardly has any sense. Therefore, we do not consider it here.

6. Conclusions

We analyzed the sensitivity of squeezing-enhanced interferometers using the unified approach based on the convenient uncertainty-relation-type form of QCRB, presented in Section 3.1. We considered both linear (SU(2)) and non-linear (SU(1,1)) interferometers, as well as the hybrid SU(2)/SU(1,1) schemes, taking into account the practical limitations of all real-world high-sensitive interferometers. In particular, we assumed the realistic case of Gaussian states of the probing light, supplemented by the strong classical carrier, see the condition (7).

We focused on the following three configurations, defined by the interferometer symmetry: (i) the *asymmetric* single-arm interferometer; (ii) the symmetric two-arm interfer-

ometer with the *antisymmetric* phase shifts in the arms, and (iii) the symmetric two-arm interferometer with the *symmetric* phase shifts in the arms.

We showed that while the optimal regimes for these cases differ significantly, the QCRBs for both linear (SU(2)) and non-linear (SU(1,1)) interferometers are given by the following equations having the same uniform structure that first appeared in the work [10].

In the asymmetric case of the single-arm (both SU(2) and SU(1,1)) interferometers,

$$\langle (\delta\phi)^2 \rangle \geq \frac{e^{-2r}}{4\mathcal{N}}, \quad (104)$$

where

$$\mathcal{N} = N + o(N), \quad (105)$$

N is the mean number of photons at the phase-shifting object, and r is the corresponding squeeze factor. The function $o(N)$ is defined in the standard way: $o(N)/N \rightarrow 0$ if $N \rightarrow \infty$.

In the case of the two-arm SU(2) interferometer, the sensitivity for the symmetric and antisymmetric phase shifts depends on the squeeze factors r_1 and r_2 at the bright and dark ports, respectively:

$$\langle (\delta\phi_+)^2 \rangle \geq \frac{e^{-2r_1}}{4\mathcal{N}}, \quad (106a)$$

$$\langle (\delta\phi_-)^2 \rangle \geq \frac{e^{-2r_2}}{4\mathcal{N}}, \quad (106b)$$

where \mathcal{N} is still defined by Equation (105), but with N being the total photon number in the both arms.

In principle, the input part of the SU(2) interferometer (the input beamsplitter + squeezer(s)) can be replaced by the SU(1,1) type one, that is, by the single non-degenerate optical parametric amplifier with the squeeze factor r . This configuration gives the QCRB, which also is described by Equation (106), but with $-r_1 = r_2$.

In the ideal lossless case, the standard measurement schemes, namely the direct detection and, if the additional phase reference is available, the homodyne detection, allow to asymptotically (that is, for the case of $N \gg 1$) saturate these limits. In presence of the optical losses, the general structure of Equations (104) and (106) still holds up to the replacement of the squeeze factors by the effective lossy ones following the rule (4).

We have to mention also that the two-arm interferometers, the SU(1,1) type detection scheme (the non-degenerate optical parametric amplifier followed by the photodetector(s)) hardly has any sense because it gives information on ϕ_+ only; therefore, a single-arm interferometer would be sufficient for this case.

Author Contributions: Conceptualization, F.K.; investigation, D.S. and F.K.; writing—original draft preparation, D.S. and F.K.; writing—review and editing, D.S. and F.K. All authors have read and agreed to the published version of the manuscript.

Funding: The work of F.K. was supported by the Russian Foundation for Basic Research grant 19-29-11003.

Conflicts of Interest: The authors declare no conflict of interest.

Abbreviations

The following abbreviations are used in this manuscript:

SNL	Shot noise limit
HL	Heisenberg limit
QCRB	Quantum Cramèr–Rao bound
OPA	Optical parametric amplifier
DOPA	Degenerate optical parametric amplifier
NOPA	Non-degenerate optical parametric amplifier

Appendix A. Fisher Information Matrix

Using Equations (16)–(20), Equation (15) can be presented as follows:

$$i(\hat{\rho}\hat{N}_j - \hat{N}_j\hat{\rho}) = \frac{1}{2}(\hat{\rho}\hat{L}_j + \hat{L}_j\hat{\rho}). \tag{A1}$$

Let $|\rho_l\rangle, p_l$ be the eigenstates and eigenvalues of ρ :

$$\hat{\rho} = \sum_l |\rho_l\rangle p_l \langle \rho_l|. \tag{A2}$$

Using this representation, Equation (15) can be solved explicitly:

$$\langle \rho_l | \hat{L}_j | \rho_m \rangle = 2i \frac{p_l - p_m}{p_l + p_m} \langle \rho_l | \hat{N}_j | \rho_m \rangle. \tag{A3}$$

Substitution of this solution into Equation (14) gives:

$$\begin{aligned} \mathbb{A}_{jk} &= \frac{1}{2} \sum_{lm} p_l \left(\langle \rho_l | \hat{L}_j | \rho_m \rangle \langle \rho_m | \hat{L}_k | \rho_l \rangle + \langle \rho_l | \hat{L}_k | \rho_m \rangle \langle \rho_m | \hat{L}_j | \rho_l \rangle \right) \\ &= 2 \sum_{lm} \frac{(p_l - p_m)^2}{p_l + p_m} \langle \rho_l | \hat{N}_j | \rho_m \rangle \langle \rho_m | \hat{N}_k | \rho_l \rangle. \end{aligned} \tag{A4}$$

Suppose that $\hat{\rho}$ is a pure state:

$$p_0 = 1, \quad p_{l \neq 0} = 0. \tag{A5}$$

In this case, only the terms with $l = 0, m \neq 0$ and $l \neq 0, m = 0$ survive in Equation (A4):

$$\begin{aligned} \mathbb{A}_{jk} &= 2 \left(\sum_{m \neq 0} \langle \rho_0 | \hat{N}_j | \rho_m \rangle \langle \rho_m | \hat{N}_k | \rho_0 \rangle + \sum_{l \neq 0} \langle \rho_l | \hat{N}_j | \rho_0 \rangle \langle \rho_0 | \hat{N}_k | \rho_l \rangle \right) \\ &= 4(\langle \hat{N}_j \hat{N}_k \rangle - \langle \hat{N}_j \rangle \langle \hat{N}_k \rangle) = 4\langle \delta \hat{N}_j \delta \hat{N}_k \rangle. \end{aligned} \tag{A6}$$

Appendix B. Single-Arm Interferometer with SU(1,1) Measurement

Evolution of the optical field in the single-arm SU(1,1) interferometer shown in Figure 4a is described by Equations (28), (41) and (43). It follows from these equations that

$$\hat{d} = \sqrt{\eta}(B\hat{\alpha} + C\hat{z} + S\hat{z}^\dagger) + \sqrt{1-\eta}\hat{y}, \tag{A7}$$

where

$$B = e^{-i\phi} \cosh R - e^{2i\theta+i\phi} \sinh R, \tag{A8a}$$

$$C = e^{-i\phi} \cosh r \cosh R - e^{i\phi} \sinh r \sinh R, \tag{A8b}$$

$$S = e^{2i\theta-i\phi} \sinh r \cosh R - e^{2i\theta+i\phi} \cosh r \sinh R. \tag{A8c}$$

Therefore, the mean value and variance of $\hat{n} = \hat{f}^\dagger \hat{f}$ are equal to

$$\langle \hat{n} \rangle = \eta(|B|^2\alpha^2 + |S|^2), \tag{A9a}$$

$$\langle (\delta \hat{n})^2 \rangle = \eta^2 [|B^*S + BC^*|^2\alpha^2 + 2|C|^2|S|^2 + \epsilon^2(|B|^2\alpha^2 + |S|^2)]. \tag{A9b}$$

In the particular case of (44),

$$B = \frac{e^R}{2}(e^{-i\phi} - e^{2i\theta+i\phi}), \tag{A10a}$$

$$C = \frac{e^R}{2}\sigma, \tag{A10b}$$

$$S = -\frac{e^R}{2}e^{2i\theta}\sigma^*, \tag{A10c}$$

where

$$\sigma = e^{-i\phi} \cosh r - e^{i\phi} \sinh r, \tag{A11}$$

which gives Equation (45).

Appendix C. Variances of the Photon Numbers in the Arms of the SU(2) Interferometer

It follows from Equation (54) that

$$\delta(\hat{a}_j^\dagger \hat{a}_j)|0\rangle = [(\alpha_j G_j + \alpha_j^* g_j)\hat{z}_j^\dagger + G_j g_j \hat{z}_j^{\dagger 2}]|0\rangle, \tag{A12a}$$

$$\delta(\hat{a}_1^\dagger \hat{a}_2)|0\rangle = (\alpha_2 G_1 \hat{z}_1^\dagger + \alpha_1^* g_2 \hat{z}_2^\dagger + G_1 g_2 \hat{z}_1^\dagger \hat{z}_2^\dagger)|0\rangle, \tag{A12b}$$

$$\delta(\hat{a}_2^\dagger \hat{a}_1)|0\rangle = (\alpha_1 G_2 \hat{z}_2^\dagger + \alpha_2^* g_1 \hat{z}_1^\dagger + G_2 g_1 \hat{z}_1^\dagger \hat{z}_2^\dagger)|0\rangle, \tag{A12c}$$

and

$$\delta\hat{N}_+|0\rangle = \sum_{j=1,2} (A_{jj}\hat{z}_j^\dagger + G_j g_j \hat{z}_j^{\dagger 2})|0\rangle, \tag{A13a}$$

$$\delta\hat{N}_-|0\rangle = [A_{21}\hat{z}_1^\dagger + A_{12}\hat{z}_2^\dagger + (G_1 g_2 + G_2 g_1)\hat{z}_1^\dagger \hat{z}_2^\dagger]|0\rangle, \tag{A13b}$$

where

$$G_j = \cosh r_j, \quad g_j = e^{2i\theta_j} \sinh r_j, \tag{A14}$$

$$A_{jk} = \alpha_j G_k + \alpha_j^* g_k. \tag{A15}$$

Therefore,

$$\langle(\delta\hat{N}_+)^2\rangle = \sum_{j=1,2} (|A_{jj}|^2 + 2G_j^2 |g_j|^2), \tag{A16a}$$

$$\langle(\delta\hat{N}_-)^2\rangle = |A_{21}|^2 + |A_{12}|^2 + |G_1 g_2 + G_2 g_1|^2, \tag{A16b}$$

$$\langle\delta\hat{N}_+ \delta\hat{N}_-\rangle = A_{11}^* A_{21} + A_{22}^* A_{12}. \tag{A16c}$$

With account for the conditions (58), Equation (A16) reduce to Equation (61).

Appendix D. Measurement Error in the Double Direct Detection Case

Equation (87) give that

$$\hat{n}_1|0\rangle = (\alpha^2 + \alpha\hat{z}_1^\dagger e^{r_1} + \hat{z}_1^{\dagger 2} \cosh r_1 \sinh r_1 + \sinh^2 r_1)|0\rangle, \tag{A17a}$$

$$\hat{n}_2|0\rangle = (\hat{z}_2^{\dagger 2} \cosh r_2 \sinh r_2 + \sinh^2 r_2)|0\rangle, \tag{A17b}$$

$$\hat{Y}|0\rangle = i[\alpha\hat{z}_2^\dagger e^{-r_2} + \hat{z}_1^\dagger \hat{z}_2^\dagger \sinh(r_1 - r_2)]|0\rangle. \tag{A17c}$$

Therefore,

$$\langle\hat{n}_1\rangle = \alpha^2 + \sinh^2 r_1, \tag{A18a}$$

$$\langle\hat{n}_2\rangle = \sinh^2 r_2, \tag{A18b}$$

$$\langle Y\rangle = 0, \tag{A18c}$$

$$\langle(\delta\hat{n}_1)^2\rangle = \alpha^2 e^{2r_1} + \frac{\sinh^2 2r_1}{2}, \tag{A19a}$$

$$\langle(\delta\hat{n}_2)^2\rangle = \frac{\sinh^2 2r_2}{2}, \tag{A19b}$$

$$\langle\delta\hat{n}_1 \circ \delta\hat{n}_2\rangle = 0, \tag{A19c}$$

$$\langle\hat{Y}^2\rangle = \alpha^2 e^{-2r_2} + \sinh^2(r_1 - r_2), \tag{A19d}$$

$$\langle\delta\hat{n}_1 \circ \delta\hat{Y}\rangle = \langle\delta\hat{n}_2 \circ \delta\hat{Y}\rangle = 0, \tag{A19e}$$

and

$$\langle\hat{n}_+\rangle = \alpha^2 + \sinh^2 r_1 + \sinh^2 r_2, \tag{A20a}$$

$$\langle\hat{n}_-\rangle = \alpha^2 + \sinh^2 r_1 - \sinh^2 r_2, \tag{A20b}$$

$$\langle(\delta\hat{n}_+)^2\rangle = \langle(\delta\hat{n}_-)^2\rangle = \langle(\delta\hat{n}_1)^2\rangle + \langle(\delta\hat{n}_2)^2\rangle, \tag{A21a}$$

$$\langle\delta\hat{n}_- \delta\hat{n}_+\rangle = \langle(\delta\hat{n}_1)^2\rangle - \langle(\delta\hat{n}_2)^2\rangle, \tag{A21b}$$

$$\langle\delta\hat{n}_+ \circ \delta\hat{Y}\rangle = \langle\delta\hat{n}_- \circ \delta\hat{Y}\rangle = 0. \tag{A21c}$$

where “o” denotes the symmetrized product.

Then, using Equation (96):

$$\langle\hat{n}_+^{\text{out}}\rangle = \eta\langle\hat{n}_+\rangle, \tag{A22a}$$

$$\langle\hat{n}_-^{\text{out}}\rangle = \eta\langle\hat{n}_-\rangle \cos 2\phi_-, \tag{A22b}$$

$$\langle(\delta\hat{n}_+^{\text{out}})^2\rangle = \eta^2[\langle(\delta\hat{n}_+)^2\rangle + \epsilon^2\langle\hat{n}_+\rangle] = \eta^2(\Delta_1^2 + \Delta_2^2), \tag{A23a}$$

$$\begin{aligned} \langle(\delta\hat{n}_-^{\text{out}})^2\rangle &= \eta^2[\langle(\delta\hat{n}_-)^2\rangle \cos^2 2\phi_- + \langle\hat{Y}^2\rangle \sin^2 2\phi_- + \epsilon^2\langle\hat{n}_+\rangle] \\ &= \eta^2[(\Delta_1^2 + \Delta_2^2) \cos^2 2\phi_- + (\langle\hat{Y}^2\rangle + \epsilon^2\langle\hat{n}_+\rangle) \sin^2 2\phi_-], \end{aligned} \tag{A23b}$$

$$\langle\delta\hat{n}_-^{\text{out}} \delta\hat{n}_+^{\text{out}}\rangle = \eta^2[\langle\delta\hat{n}_- \delta\hat{n}_+\rangle + \epsilon^2\langle\hat{n}_-\rangle] \cos 2\phi_- = \eta^2(\Delta_1^2 - \Delta_2^2) \cos 2\phi_-, \tag{A23c}$$

where

$$\Delta_j^2 = \langle(\delta\hat{n}_j)^2\rangle + \epsilon^2\langle\hat{n}_j\rangle. \tag{A24}$$

Substitution of Equations (A22) and (A23) into Equation (98) gives that

$$\langle(\delta\phi_-)^2\rangle = \frac{1}{4\langle n_- \rangle^2} \left(\langle\hat{Y}^2\rangle + \epsilon^2\langle\hat{n}_+\rangle + \frac{4 \cot^2 2\phi_-}{1/\Delta_1^2 + 1/\Delta_2^2} \right). \tag{A25}$$

Note that

$$\Delta_1^2 \sim \alpha^2, \quad \Delta_2^2 \sim \alpha^0. \tag{A26}$$

Therefore,

$$\begin{aligned} \langle(\delta\phi_-)^2\rangle &= \frac{1}{4\langle n_- \rangle^2} [\langle\hat{Y}^2\rangle + \epsilon^2\langle\hat{n}_+\rangle + 4\Delta_2^2 \cot^2 2\phi_- + O(\alpha^{-2})] \\ &= \frac{1}{4(\alpha^2 + \sinh^2 r_1 - \sinh^2 r_2)^2} [\alpha^2 e^{-2r_2} + \sinh^2(r_1 - r_2) + \epsilon^2(\alpha^2 + \sinh^2 r_1 + \sinh^2 r_2) \\ &\quad + 2(\sinh^2 2r_2 + 2\epsilon^2 \sinh^2 r_2) \cot^2 2\phi_- + O(\alpha^{-2})]. \end{aligned} \tag{A27}$$

References

1. Michelson, A.; Morley, E. On the Relative Motion of the Earth and the Luminiferous Ether. *Am. J. Sci. Ser.* **1887**, *34*, 333–345. [[CrossRef](#)]
2. Abbott, B.P.; Abbott, R.; Abbott, T.D.; Abernathy, M.R.; Acernese, F.; Ackley, K.; Adams, C.; Adams, T.; Addesso, P.; Adhikari, R.X.; et al. Observation of Gravitational Waves from a Binary Black Hole Merger. *Phys. Rev. Lett.* **2016**, *116*, 061102. [[CrossRef](#)]
3. Laser Interferometer Gravitational-Wave Observatory (LIGO). Available online: <https://www.ligo.caltech.edu> (accessed on 10 January 2023).
4. Virgo Collaboration. Available online: <http://www.virgo-gw.eu> (accessed on 10 January 2023).
5. Tse, M.E.; Yu, H.; Kijbunchoo, N.; Fernandez-Galiana, A.; Dupej, P.; Barsotti, L.; Blair, C.D.; Brown, D.D.; Dwyer, S.E.; Effler, A.; et al. Quantum-Enhanced Advanced LIGO Detectors in the Era of Gravitational-Wave Astronomy. *Phys. Rev. Lett.* **2019**, *123*, 231107. [[CrossRef](#)]
6. Aasi, J.; Abbott, B.P.; Abbott, R.; Abbott, T.; Abernathy, M.R.; Ackley, K.; Adams, C.; Adams, T.; Addesso, P.; Adhikari, R.X.; et al. Advanced LIGO. *Class. Quantum Gravity* **2015**, *32*, 074001.
7. Richardson, J.W.; Pandey, S.; Bytyqi, E.; Edo, T.; Adhikari, R.X. Optimizing Gravitational-Wave Detector Design for Squeezed Light. *Phys. Rev. D* **2022**, *105*, 10200. [[CrossRef](#)]
8. Taylor, M.A.; Bowen, W.P. Quantum metrology and its application in biology. *Phys. Rep.* **2016**, *615*, 1–59. [[CrossRef](#)]
9. Yuen, H.P. Two-photon coherent states of the radiation field. *Phys. Rev. A* **1976**, *13*, 2226–2243. [[CrossRef](#)]
10. Caves, C.M. Quantum-mechanical noise in an interferometer. *Phys. Rev. D* **1981**, *23*, 1693–1708. [[CrossRef](#)]
11. Holland, M.J.; Burnett, K. Interferometric detection of optical phase shifts at the Heisenberg limit. *Phys. Rev. Lett.* **1993**, *71*, 1355–1358. [[CrossRef](#)]
12. Lane, A.S.; Braunstein, S.L.; Caves, C.M. Maximum-likelihood statistics of multiple quantum phase measurements. *Phys. Rev. A* **1993**, *47*, 1667–1696. [[CrossRef](#)]
13. Sanders, B.C.; Milburn, G.J.; Zhang, Z. Optimal quantum measurements for phase-shift estimation in optical interferometry. *J. Mod. Opt.* **1997**, *44*, 1309–1320. [[CrossRef](#)]
14. Demkowicz-Dobrzański, R.; Kołodyński, J.; Guţă, M. The elusive Heisenberg limit in quantum-enhanced metrology. *Nat. Commun.* **2012**, *3*, 1063. [[CrossRef](#)]
15. Pezzè, L.; Hyllus, P.; Smerzi, A. Phase-sensitivity bounds for two-mode interferometers. *Phys. Rev. A* **2015**, *91*, 032103. [[CrossRef](#)]
16. Manceau, M.; Khalili, F.; Chekhova, M. Improving the phase super-sensitivity of squeezing-assisted interferometers by squeeze factor unbalancing. *New J. Phys.* **2017**, *19*, 013014. [[CrossRef](#)]
17. Gessner, M.; Pezzè, L.; Smerzi, A. Sensitivity Bounds for Multiparameter Quantum Metrology. *Phys. Rev. Lett.* **2018**, *121*, 130503. [[CrossRef](#)] [[PubMed](#)]
18. Pezzè, L.; Smerzi, A. Ultrasensitive Two-Mode Interferometry with Single-Mode Number Squeezing. *Phys. Rev. Lett.* **2013**, *110*, 163604. [[CrossRef](#)] [[PubMed](#)]
19. Campos, R.A.; Gerry, C.C.; Benmoussa, A. Optical interferometry at the Heisenberg limit with twin Fock states and parity measurements. *Phys. Rev. A* **2003**, *68*, 023810. [[CrossRef](#)]
20. Kumar, C.; Rishabh; Sharma, M.; Arora, S. Parity-detection-based Mach–Zehnder interferometry with coherent and non-Gaussian squeezed vacuum states as inputs. *arXiv* **2022**, arXiv:2212.12421.
21. Zhao, Z.; Zhang, H.; Huang, Y.; Hu, L. Phase estimation of Mach–Zehnder interferometer via Laguerre excitation squeezed state. *arXiv* **2022**, arXiv:2209.00338.
22. Lee, H.; Kok, P.; Dowling, J.P. A quantum Rosetta stone for interferometry. *J. Mod. Opt.* **2002**, *49*, 2325–2338. [[CrossRef](#)]
23. Berry, D.W.; Higgins, B.L.; Bartlett, S.D.; Mitchell, M.W.; Pryde, G.J.; Wiseman, H.M. How to perform the most accurate possible phase measurements. *Phys. Rev. A* **2009**, *80*, 052114. [[CrossRef](#)]
24. Perarnau-Llobet, M.; González-Tudela, A.; Cirac, J.I. Multimode Fock states with large photon number: Effective descriptions and applications in quantum metrology. *Quantum Sci. Technol.* **2020**, *5*, 025003. [[CrossRef](#)]
25. Akhtar, N.; Sanders, B.C.; Xianlong, G. Sub-Planck phase-space structure and sensitivity for SU(1,1) compass states. *Phys. Rev. A* **2022**, *106*, 043704. [[CrossRef](#)]
26. Demkowicz-Dobrzański, R.; Jarzyna, M.; Kolodyński, J. Chapter Four—Quantum Limits in Optical Interferometry. *Prog. Opt.* **2015**, *60*, 345–435. [[CrossRef](#)]
27. Barbieri, M. Optical Quantum Metrology. *PRX Quantum* **2022**, *3*, 010202. [[CrossRef](#)]
28. Daryanoosh, S.; Slussarenko, S.; Berry, D.W.; Wiseman, H.M.; Pryde, G.J. Experimental optical phase measurement approaching the exact Heisenberg limit. *Nat. Commun.* **2018**, *9*, 4606. [[CrossRef](#)]
29. Lang, M.D.; Caves, C.M. Optimal Quantum-Enhanced Interferometry Using a Laser Power Source. *Phys. Rev. Lett.* **2013**, *111*, 173601. [[CrossRef](#)]
30. Lang, M.D.; Caves, C.M. Optimal quantum-enhanced interferometry. *Phys. Rev. A* **2014**, *90*, 025802. [[CrossRef](#)]
31. Xiao, M.; Wu, L.A.; Kimble, H.J. Precision measurement beyond the shot-noise limit. *Phys. Rev. Lett.* **1987**, *59*, 278–281. [[CrossRef](#)] [[PubMed](#)]
32. Grangier, P.; Slusher, R.E.; Yurke, B.; LaPorta, A. Squeezed-light-enhanced polarization interferometer. *Phys. Rev. Lett.* **1987**, *59*, 2153–2156. [[CrossRef](#)]

33. Eberle, T.; Steinlechner, S.; Bauchrowitz, J.; Händchen, V.; Vahlbruch, H.; Mehmet, M.; Müller-Ebhardt, H.; Schnabel, R. Quantum Enhancement of the Zero-Area Sagnac Interferometer Topology for Gravitational Wave Detection. *Phys. Rev. Lett.* **2010**, *104*, 251102. [[CrossRef](#)] [[PubMed](#)]
34. Vahlbruch, H.; Mehmet, M.; Danzmann, K.; Schnabel, R. Detection of 15 dB Squeezed States of Light and their Application for the Absolute Calibration of Photoelectric Quantum Efficiency. *Phys. Rev. Lett.* **2016**, *117*, 110801. [[CrossRef](#)]
35. Frascella, G.; Agne, S.; Khalili, F.Y.; Chekhova, M.V. Overcoming detection loss and noise in squeezing-based optical sensing. *NPJ Quantum Inf.* **2021**, *7*, 72. [[CrossRef](#)]
36. Zander, J. Squeezed and Entangled Light: From Foundations of Quantum Mechanics to Quantum Sensing. Ph.D. Thesis, Universität Hamburg, Hamburg, Germany, 2021.
37. Mehmet, M.; Vahlbruch, H. High-efficiency squeezed light generation for gravitational wave detectors. *Class. Quantum Gravity* **2018**, *36*, 015014. [[CrossRef](#)]
38. Pradyumna, S.T.; Losero, E.; Ruo-Berchera, I.; Traina, P.; Zucco, M.; Jacobsen, C.S.; Andersen, U.L.; Degiovanni, I.P.; Genovese, M.; Gehring, T. Twin beam quantum-enhanced correlated interferometry for testing fundamental physics. *Commun. Phys.* **2020**, *3*, 104. [[CrossRef](#)]
39. Zuo, X.; Yan, Z.; Feng, Y.; Ma, J.; Jia, X.; Xie, C.; Peng, K. Quantum Interferometer Combining Squeezing and Parametric Amplification. *Phys. Rev. Lett.* **2020**, *124*, 173602. [[CrossRef](#)]
40. Darsow-Fromm, C.; Gurs, J.; Schnabel, R.; Steinlechner, S. Squeezed light at 2128 nm for future gravitational-wave observatories. *Opt. Lett.* **2021**, *46*, 5850–5853. [[CrossRef](#)] [[PubMed](#)]
41. Heinze, J.; Danzmann, K.; Willke, B.; Vahlbruch, H. 10 dB Quantum-Enhanced Michelson Interferometer with Balanced Homodyne Detection. *Phys. Rev. Lett.* **2022**, *129*, 031101. [[CrossRef](#)]
42. Abadie, J.; Abbott, B.P.; Abbott, R.; Abbott, T.D.; Abernathy, M.; Adams, C.; Adhikari, R.; Affeldt, C.; Allen, B.; Allen, G. S.; et al. A gravitational wave observatory operating beyond the quantum shot-noise limit. *Nat. Phys.* **2011**, *7*, 962–965. [[CrossRef](#)]
43. Acernese, F.; Agathos, M.; Aiello, L.; Allocca, A.; Amato, A.; Ansoldi, S.; Antier, S.; Arène, M.; Arnaud, N.; Ascenzi, S.; et al. Increasing the Astrophysical Reach of the Advanced Virgo Detector via the Application of Squeezed Vacuum States of Light. *Phys. Rev. Lett.* **2019**, *123*, 231108. [[CrossRef](#)]
44. Schnabel, R. Squeezed states of light and their applications in laser interferometers. *Phys. Rep.* **2017**, *684*, 1–51. [[CrossRef](#)]
45. Punturo, M.; Abernathy, M.; Acernese, F.; Allen, B.; Andersson, N.; Arun, K.; Barone, F.; Barr, B.; Barsuglia, M.; Beker, M.; et al. The Einstein Telescope: A third-generation gravitational wave observatory. *Class. Quantum Gravity* **2010**, *27*, 194002. [[CrossRef](#)]
46. Reitze, D.; Adhikari, R.X.; Ballmer, S.; Barish, B.; Barsotti, L.; Billingsley, G.; Brown, D.A.; Chen, Y.; Coyne, D.; Eisenstein, R.; et al. Cosmic Explorer: The U.S. Contribution to Gravitational-Wave Astronomy beyond LIGO. *arXiv* **2019**, arXiv:1907.04833.
47. Zurek, W.H. Decoherence, einselection, and the quantum origins of the classical. *Rev. Mod. Phys.* **2003**, *75*, 715–775. [[CrossRef](#)]
48. Demkowicz-Dobrzański, R.; Banaszek, K.; Schnabel, R. Fundamental quantum interferometry bound for the squeezed-light-enhanced gravitational wave detector GEO 600. *Phys. Rev. A* **2013**, *88*, 041802. [[CrossRef](#)]
49. Yurke, B.; McCall, S.L.; Klauder, J.R. SU(2) and SU(1,1) interferometers. *Phys. Rev. A* **1986**, *33*, 4033–4054. [[CrossRef](#)] [[PubMed](#)]
50. Ataman, S.; Preda, A.; Ionicioiu, R. Phase sensitivity of a Mach–Zehnder interferometer with single-intensity and difference-intensity detection. *Phys. Rev. A* **2018**, *98*, 043856. [[CrossRef](#)]
51. Ataman, S. Optimal Mach–Zehnder phase sensitivity with Gaussian states. *Phys. Rev. A* **2019**, *100*, 063821. [[CrossRef](#)]
52. Ataman, S. Single- versus two-parameter Fisher information in quantum interferometry. *Phys. Rev. A* **2020**, *102*, 013704. [[CrossRef](#)]
53. Mishra, K.K.; Ataman, S. Optimal phase sensitivity of an unbalanced Mach–Zehnder interferometer. *Phys. Rev. A* **2022**, *106*, 023716. [[CrossRef](#)]
54. Andersen, U.L.; Glöckl, O.; Gehring, T.; Leuchs, G., Quantum Interferometry with Gaussian States. In *Quantum Information*; John Wiley & Sons, Ltd.: Hoboken, NJ, USA, 2019; Chapter 35, pp. 777–798. [[CrossRef](#)]
55. Du, W.; Jia, J.; Chen, J.F.; Ou, Z.Y.; Zhang, W. Absolute sensitivity of phase measurement in an SU(1,1) type interferometer. *Opt. Lett.* **2018**, *43*, 1051–1054. [[CrossRef](#)]
56. Frascella, G.; Mikhailov, E.E.; Takanashi, N.; Zakharov, R.V.; Tikhonova, O.V.; Chekhova, M.V. Wide-field SU(1,1) interferometer. *Optica* **2019**, *6*, 1233–1236. [[CrossRef](#)]
57. Plick, W.N.; Dowling, J.P.; Agarwal, G.S. Coherent-light-boosted, sub-shot noise, quantum interferometry. *New J. Phys.* **2010**, *12*, 083014. [[CrossRef](#)]
58. Ferreri, A.; Santandrea, M.; Stefszky, M.; Luo, K.H.; Herrmann, H.; Silberhorn, C.; Sharapova, P.R. Spectrally multimode integrated SU(1,1) interferometer. *Quantum* **2021**, *5*, 461. [[CrossRef](#)]
59. Ye, W.; Chang, S.K.; Gao, S.Y.; Zhang, H.; Xia, Y.; Rao, X. Quantum-improved phase estimation with a displacement-assisted SU(1,1) interferometer. *arXiv* **2022**, arXiv:2210.02645.
60. Flórez, J.; Pearce, E.; Gemmell, N.R.; Ma, Y.; Bressanini, G.; Phillips, C.C.; Oulton, R.F.; Clark, A.S. Enhanced nonlinear interferometry via seeding. *arXiv* **2022**, arXiv:2209.06749.
61. Thekkadath, G.S.; Mycroft, M.E.; Bell, B.A.; Wade, C.G.; Eckstein, A.; Phillips, D.S.; Patel, R.B.; Buraczewski, A.; Lita, A.E.; Gerrits, T.; et al. Quantum-enhanced interferometry with large heralded photon-number states. *NPJ Quantum Inf.* **2020**, *6*, 89. [[CrossRef](#)] [[PubMed](#)]

62. Anderson, B.E.; Gupta, P.; Schmittberger, B.L.; Horrom, T.; Hermann-Avigliano, C.; Jones, K.M.; Lett, P.D. Phase sensing beyond the standard quantum limit with a variation on the SU(1,1) interferometer. *Optica* **2017**, *4*, 752–756. [[CrossRef](#)]
63. Seyfarth, U.; Klimov, A.B.; Guise, H.d.; Leuchs, G.; Sanchez-Soto, L.L. Wigner function for SU(1,1). *Quantum* **2020**, *4*, 317. [[CrossRef](#)]
64. Schleich, W.. *Quantum Optics in Phase Space*; WILEY-VCH: Berlin, Germany, 2001; p. 695.
65. Luo, K.H.; Santandrea, M.; Stefszky, M.; Sperling, J.; Massaro, M.; Ferreri, A.; Sharapova, P.R.; Herrmann, H.; Silberhorn, C. Quantum optical coherence: From linear to nonlinear interferometers. *Phys. Rev. A* **2021**, *104*, 043707. [[CrossRef](#)]
66. Chekhova, M.V.; Ou, Z.Y. Nonlinear interferometers in quantum optics. *Adv. Opt. Photon.* **2016**, *8*, 104–155. [[CrossRef](#)]
67. Ou, Z.Y.; Li, X. Quantum SU(1,1) interferometers: Basic principles and applications. *APL Photonics* **2020**, *5*, 080902. [[CrossRef](#)]
68. Liang, X.; Yu, Z.; Yuan, C.H.; Zhang, W.; Chen, L. Phase Sensitivity Improvement in Correlation-Enhanced Nonlinear Interferometers. *Symmetry* **2022**, *14*, 2684. [[CrossRef](#)]
69. Helstrom, C.W. *Quantum Detection and Estimation Theory*; Academic Press: New York, NY, USA, 1976; p. 309.
70. Heitler, W. *The Quantum Theory of Radiation*, 3rd ed.; Clarendon Press: Oxford, UK, 1954.
71. Susskind, L.; Glogower, J. Quantum mechanical phase and time operator. *Phys. Phys. Fiz.* **1964**, *1*, 49–61. [[CrossRef](#)]
72. Carruthers, P.; Nieto, M.M. Phase and Angle Variables in Quantum Mechanics. *Rev. Mod. Phys.* **1968**, *40*, 411–440. [[CrossRef](#)]
73. Carruthers, P.; Nieto, M.M. Coherent States and the Number-Phase Uncertainty Relation. *Phys. Rev. Lett.* **1965**, *14*, 387–389. [[CrossRef](#)]
74. Pegg, D.T.; Barnett, S.M. Phase properties of the quantized single-mode electromagnetic field. *Phys. Rev. A* **1989**, *39*, 1665–1675. [[CrossRef](#)]
75. Fresneda, R.; Gazeau, J.P.; Noguera, D. Quantum localisation on the circle. *J. Math. Phys.* **2018**, *59*, 052105. [[CrossRef](#)]
76. Aasi, J.; Abadie, J.; Abbott, B.P.; Abbott, R.; Abbott, T.D.; Abernathy, M.R.; Adams, C.; Adams, T.; Addesso, P.; Adhikari, R.X.; et al. Enhanced sensitivity of the LIGO gravitational wave detector by using squeezed states of light. *Nat. Photonics* **2013**, *7*, 613–619. [[CrossRef](#)]
77. Jarzyna, M.; Demkowicz-Dobrzański, R. Quantum interferometry with and without an external phase reference. *Phys. Rev. A* **2012**, *85*, 011801. [[CrossRef](#)]
78. Müller-Ebhardt, H.; Rehbein, H.; Schnabel, R.; Danzmann, K.; Chen, Y. Entanglement of Macroscopic Test Masses and the Standard Quantum Limit in Laser Interferometry. *Phys. Rev. Lett.* **2008**, *100*, 013601. [[CrossRef](#)]
79. Müller-Ebhardt, H.; Rehbein, H.; Li, C.; Mino, Y.; Somiya, K.; Schnabel, R.; Danzmann, K.; Chen, Y. Quantum-state preparation and macroscopic entanglement in gravitational-wave detectors. *Phys. Rev. A* **2009**, *80*, 043802. [[CrossRef](#)]
80. Schnabel, R. Einstein-Podolsky-Rosen-entangled motion of two massive objects. *Phys. Rev. A* **2015**, *92*, 012126. [[CrossRef](#)]
81. Takeoka, M.; Seshadreesan, K.P.; You, C.; Izumi, S.; Dowling, J.P. Fundamental precision limit of a Mach–Zehnder interferometric sensor when one of the inputs is the vacuum. *Phys. Rev. A* **2017**, *96*, 052118. [[CrossRef](#)]
82. Hofmann, H.F. All path-symmetric pure states achieve their maximal phase sensitivity in conventional two-path interferometry. *Phys. Rev. A* **2009**, *79*, 033822. [[CrossRef](#)]
83. Leonhardt, U.; Paul, H. Realistic optical homodyne measurements and quasiprobability distributions. *Phys. Rev. A* **1993**, *48*, 4598–4604. [[CrossRef](#)]
84. Pezzé, L.; Smerzi, A. Mach–Zehnder Interferometry at the Heisenberg Limit with Coherent and Squeezed-Vacuum Light. *Phys. Rev. Lett.* **2008**, *100*, 073601. [[CrossRef](#)]
85. Manceau, M.; Leuchs, G.; Khalili, F.; Chekhova, M. Detection Loss Tolerant Supersensitive Phase Measurement with an SU(1,1) Interferometer. *Phys. Rev. Lett.* **2017**, *119*, 223604. [[CrossRef](#)]
86. Danilishin, S.L.; Khalili, F.Y. Quantum Measurement Theory in Gravitational-Wave Detectors. *Living Rev. Relativ.* **2012**, *15*, 5. [[CrossRef](#)]
87. Danilishin, S.L.; Khalili, F.Y.; Miao, H. Advanced quantum techniques for future gravitational-wave detectors. *Living Rev. Relativ.* **2019**, *22*, 2. [[CrossRef](#)]
88. Shukla, G.; Salykina, D.; Frascella, G.; Mishra, D.K.; Chekhova, M.V.; Khalili, F.Y. Broadening the high sensitivity range of squeezing-assisted interferometers by means of two-channel detection. *Opt. Express* **2021**, *29*, 95–104. [[CrossRef](#)]

Disclaimer/Publisher’s Note: The statements, opinions and data contained in all publications are solely those of the individual author(s) and contributor(s) and not of MDPI and/or the editor(s). MDPI and/or the editor(s) disclaim responsibility for any injury to people or property resulting from any ideas, methods, instructions or products referred to in the content.